Environment Canada

Environnement Canada

National Water Research Institute

Institut National de Recherche sur les Eaux

THE SEASONAL CLIMATE OF THE UPPER OCEAN: DATA ANALYSIS AND MODEL DEVELOPMENT

by

T.J. Simons

THE SEASONAL CLIMATE OF THE UPPER OCEAN: DATA ANALYSIS AND MODEL DEVELOPMENT

by

T.J. Simons

THE SEASONAL CLIMATE OF THE UPPER OCEAN: DATA ANALYSIS AND MODEL DEVELOPMENT

by

T.J. Simons

National Water Research Institute
BURLINGTON, Ontario, L7R 4A6

in cooperation with

Canadian Climate Centre
DOWNSVIEW, Ontario

Interim Report
March 1981

ABSTRACT

This report describes the design and verification of an upper ocean stratification model suitable for coupling with an atmospheric general circulation model at seasonal time scales. The model is based on turbulence closure principles and is initially evaluated by recourse to detailed temperature observations and heat budgets available for Lake Ontario. Heat budgets for the northern hemisphere oceans are computed and the results are used to incorporate Ekman pumping and large scale advective effects into the model.

A series of model experiments is carried out to evaluate the sensitivity of the model to the turbulence closure parameters and to the annual mean and seasonal components of surface heating, Ekman pumping, and other advective effects. It is concluded that adequate simulation of seasonal variations of sea surface temperatures may be achieved by the simplest type of model responding only to the seasonal component of surface heating and excluding all advective effects.

1 INTRODUCTION

A striking aspect of the combined ocean-atmosphere system is the apparent incongruity of the characteristic time and space scales of the respective sub-systems. Whereas the atmospheric adjustment time is shorter than one year, the deep ocean may take more than one hundred years to reach an equilibrium state. And, while a spatial resolution of a few hundred kilometers appears acceptable for atmospheric models, a resolution of a few tens of kilometers is required to resolve the most interesting phenomena in the oceans such as eddies, coastal currents and upwelling. The coupling of an oceanic model with an atmospheric GCM (general circulation model) is therefore not a straightforward matter (Bryan et al., 1975).

On the other hand, the processes at the ocean surface are among the most imporant feedback mechanisms to be included in a realistic climate model. It is estimated that the oceans carry nearly as much heat from the equator to the poles as the atmosphere itself (Oort and VonderHaar, 1975). The oceans are the basic source of latent heat, the transport of which constitutes about one-half of the total poleward heat transport in the atmosphere. The large thermal capacity of the ocean leads to a considerable reduction of seasonal climate variations. In particular, there is the dynamic coupling of atmospheric winds and ocean currents and the direct interaction between air and water temperatures at the sea surface.

The above leads to the conclusion that any climatic GCM must include some form of oceanic component but that the latter should be tailored to the specific space and time scales of interest. The present study is concerned with interactions of oceans and atmosphere at global space scales and seasonal time scales. The principal purpose of the oceanic model component then is to provide the annual cycle of

the SST (sea surface temperature) under influence of atmospheric inputs of heat and momentum. Seasonal temperature variations in the oceans are confined to the upper few hundred meters. It would seem practical, therefore, to try and model this seasonal layer without including a complete description of the deep ocean. Thus, the problem of the long adjustment time of the deep ocean may be avoided by using climatological mean conditions below the seasonal layer.

Although the annual temperature cycle appears confined to the seasonal upper layer, this does not imply that only the upper ocean responds to seasonal variations in atmospheric forcing. In fact, it was shown by Veronis and Stommel (1956) that the response of mid-latitude oceans to short period forcing tends to be barotropic rather than baroclinic and hence the circulation of the deep ocean must be expected to vary at these time scales. Such effects may be explicitly accounted for in a model of the seasonal layer by imbedding the latter in a relatively course three-dimensional ocean model as done, for example, by Kim and Gates (1979). These authors suggest, in fact, that large scale temperature advection cannot be ignored in considering seasonal fluctuations of the SST on a global scale.

Gill and Niiler (1973) analyzed the seasonal heat balance of the upper ocean and concluded that away from the equator an approximate local balance should exist between the rate of heat storage and seasonal deviations of surface heating from the annual mean. Their results suggest that geostrophic advection is negligible but that there may be a small contribution from wind-driven Ekman currents. Wells (1979) incorporated this effect into a seasonal upper ocean model which was forced by an atmospheric GCM. He concluded that the heat storage was strongly affected by Ekman advection but it appears that he computed total instantaneous Ekman currents instead of just the seasonal components.

There is little doubt that turbulent vertical mixing of heat is the primary factor in determining the vertical temperature structure of the upper ocean and hence the SST. It is also known that one-dimensional models based on that principal (Niiler and Kraus, 1977) have now advanced to the point where they can reproduce typical annual SST cycles. Unfortunately, this is only part of the problem. If the ocean model would merely reproduce the gross features of seasonal temperture variations at the lower boundary of the atmospheric GCM, it could be replaced by prescribed climatological SST values. If, however, the purpose is to evaluate effects of air-sea interactions on the response of a coupled ocean-atmosphere system, then the problem is rather to similate deviations from normal annual cycles. This is closely related to studies of correlations between SST anomalies and atmospheric perturbations (Namias, 1972; Adem, 1975). Such anomalies are not necessarily dominated by the same physical processes which control the primary seasonal cycle as seen from the numerical experiments of Haney (1980).

Another question concerns the verification of such one-dimensional stratification models. The usual approach is to force the model by an annual cycle of surface heat flux with no net heating over the whole year and to compare the model output with cyclic temperature variations in the ocean. In particular, data from ocean weather ships have contributed greatly to model development along these lines. In the context of a climatic model, however, a major aspect of the problem is to simulate the net poleward transport of heat by the oceans over an annual cycle. In other words, there must be a net downward heat flux at the ocean surface at low latitudes and a net upward flux at high latitudes. Clearly then, a model which is perfectly tuned to a cyclic surface heating will overpredict SST's at low latitudes and underpredict them at high latitudes. Thus a crucial test of the ocean

model is to evaluate its ability to produce cyclic solutions under conditions of net surface heating and cooling.

The present report addresses the problem in two ways. First, the annual heat budget of the northern hemisphere oceans is considered by recourse to observations available in the literature. This type of calculation is not novel but it is done here to set the stage for the second part of the report. This second part deals with the design and verification of an economical and reliable upper ocean boundary layer model suitable for coupling with an atmospheric GCM. It is found that uncertainties in the data base make it difficult to judge the performance of different models, but it appears that various advective effects considered here do not lead to a systematic improvement of model results.

2 HEAT TRANSPORT EQUATION

For a study of the annual heat budget of the upper ocean, consider the heat conservation equation, ignoring small compressibility effects and any internal sources or sinks of heat.

$$\frac{\partial T}{\partial t} + \nabla\cdot(\mathbf{w}T) + \frac{\partial}{\partial z}(wT) = \frac{\partial Q}{\partial z} + \nabla\cdot\mathbf{\Gamma} \qquad (1)$$

t = time, ∇ = horizontal gradient operator, z = vertical coordinate, positive upward with origin at the sea surface, $\mathbf{w}$ = horizontal velocity vector, w = vertical velocity component, T = temperature, Q = vertical component of diffusive, sub-grid-scale, heat flux and

$\mathbb{F}$ = horizontal component of diffusive, sub-grid-scale, heat flux vector, counted positive toward decreasing x, y, z. The horizontal and vertical velocity components satisfy the quasi-incompressible continuity equation

$$\nabla\cdot\mathbf{w} + \frac{\partial w}{\partial z} = 0 \tag{2}$$

The boundary conditions at the free surface are:

$$z = \eta : w = \frac{\partial \eta}{\partial t} + \mathbf{w}\cdot\nabla\eta \; ; \; Q = Q_s \tag{3}$$

where the downward surface flux of heat at the surface, Q_s, is considered known from the surface heat balance.

Integration from the surface down to a horizontal leavel z = -h, applying the rules for interchanging integration and differentiation, and using the boundary condition (3), results in the layered equivalents of (1) and (2):

$$\frac{\partial \theta}{\partial t} + \nabla\cdot\int_{-h}^{\eta} \mathbf{v}T dz - w_h T_h = Q_s - Q_h + \nabla\cdot\mathbb{F} \tag{4}$$

$$\nabla\cdot\mathbf{V} + \frac{\partial \eta}{\partial t} = w_h \tag{5}$$

where:

$$W \equiv \int_{-h}^{\eta} w\,dz, \quad \theta \equiv \int_{-h}^{\eta} T\,dz, \quad F \equiv \int_{-h}^{\eta} \Gamma\,dz \tag{6}$$

The free surface elevation is negligible for all present purposes. The depth h is taken to be the depth of penetration of seasonal temperature variations and will be set at 250 m.

The total current, $\vec{v}$, may be separated into an inviscid component, w_i, and a frictional Ekman component, w_e, thus

$$w \equiv w_i + w_e \qquad w_h \equiv w_i + w_e \tag{7}$$

where w_e is known as the Ekman pumping. The Ekman flow is confined to a relatively thin layer near the surface; below this layer the corresponding vertical velocity will remain constant with depth and equal to w_e (ignoring bottom friction). The horizontal components of the inviscid flow will be in first approximation independent of depth within the layer of interest and the corresponding vertical velocity will increase linearly with depth in accordance with (2) until it cancels the Ekman suction at a depth H which is in general much greater than h. At the bottom of the seasonal layer, therefore, $w_i \approx (h/H)w_e \ll w_e$, which means that w_h may be replaced by w_e in (4). This approximation is similar to the assumption that, as far as the internal flow is concerned, the Ekman pumping may be applied as a boundary condition at the free surface instead of at the bottom of the Ekman layer.

If it is assumed that w_i is constant over the depth of the seasonal layer and that the Ekman layer is more or less of the same depth as the mixed layer where the temperature equals the surface

temperature T_s, then the horizontal heat transport integrated over the depth of the seasonal layer may be written as follows:

$$\int_{-h}^{\eta} wTdz = \mathbf{v}_i\theta + \mathbf{V}_e T_s \tag{8}$$

and the layered heat conservation equation becomes:

$$\frac{\partial\theta}{\partial t} = -\nabla\cdot(\mathbf{v}_i\theta) - \nabla\cdot(\mathbf{V}_e T_s) + w_e T_h + Q_s - Q_h + \nabla\cdot\mathbf{F} \tag{9}$$

To this order of approximation the inviscid current is non-divergent and hence may be represented by a streamfunction. It should be noted, however, that this holds true only for the heat conservation equation. For the dynamics, the divergence of the inviscid flow is essential because the corresponding vertical velocity must eventually cancel the Ekman suction to satisfy the boundary condition at some depth H as noted above. The continuity equation associated with (9) appears now in the following form:

$$\nabla\cdot\mathbf{v}_i = 0 \qquad \nabla\cdot\mathbf{V}_e = w_e \tag{10}$$

For the present purpose it is convenient to write the heat balance equation (9) in the following form:

$$\frac{\partial\theta}{\partial t} - Q_s = E + R \tag{11a}$$

$$E \equiv -\nabla\cdot(\mathbf{V}_e T_s) + w_e T_h \tag{11b}$$

$$R \equiv -\nabla\cdot(\mathbf{v}_i\theta) + \nabla\cdot\mathbf{F} - Q_h \tag{11c}$$

where E represents the total contribution to the heat balance of the layer due to wind-driven Ekman currents and R is the residual contribution from inviscid (mostly quasi-geostrophic) currents and diffusive processes. The sum of these two terms will be referred to as the "convergence of heat transport" whereby it is understood that such transports include horizontal and vertical advective (grid-scale) as well as diffusive (sub-grid-scale) processes. According to (11a) this convergence of heat transport equals the difference between the local rate of heat storage and the downward surface flux of heat.

It may be noted in passing that the convergence of heat transport, as defined here, is the same for the upper oceanic layer and for the whole oceanic depth, because all seasonal heat changes are presumably stored in this upper layer. This implies that the convergence of horizontal transport in the lower layer is balanced by the vertical advective and diffusive transport terms appearing in (11b and 11c).

The Ekman heat transport (11b) consists of convergence of horizontal transport in the surface layer and vertical transport through the bottom of the layer due to Ekman pumping. Alternatively, the Ekman effect may be separated into horizontal and vertical advection of heat by substituting (10) into (11b) with the result:

$$E = - \mathbf{V}_e \cdot \nabla T_s - w_e (T_s - T_h) \tag{12}$$

For the seasonal time scales under consideration, the horizontal Ekman transport integrated over the depth of the frictional layer may be obtained from the steady state relationship

$$f \mathbf{V}_e = \boldsymbol{\tau}_s \times \hat{\mathbf{k}} \tag{13}$$

where f is the Coriolis parameter, τ_s is the surface stress vector and $\hat{k}$ is the vertical unit vector. The vertical Ekman pumping follows then from (10).

The heat balance equation (11) is usually separated into the annual mean and seasonal deviations from the mean, denoted by bars and primes, respectively.

$$-\overline{Q}_s = \overline{E} + \overline{R} \tag{14a}$$

$$\frac{\partial \theta}{\partial t} - Q_s' = E' + R' \tag{14b}$$

Nonlinear terms such as the Ekman transports (12) may be computed from the total instantaneous temperatures and currents and then separated into annual and seasonal components. It is, however, of interest to expand such terms into contributions from annual and seasonal components of temperature and currents. In particular, the seasonal component of (12) becomes:

$$E' = -[\mathbb{V}_e' \cdot \nabla \overline{T}_s + w_e'(\overline{T}_s - T_h)] - [\overline{\mathbb{V}}_e \cdot \nabla T_s' + \overline{w}_e T_s'] - \varepsilon \tag{15}$$

$$\varepsilon \equiv \mathbb{V}_e' \cdot \nabla T_s' + w_e' T_s' - \overline{\mathbb{V}_e' \cdot \nabla T_s'} - \overline{w_e' T_s'}$$

where use has been made of the assumption that the temperature remains constant in time below the seasonal layer.

The various terms of (14) and (15) will be computed in the following section of this report. Before proceeding to a discussion

of the present results it is, however, useful to briefly review results of similar calculations reported in the literature.

Previous Results

Bryan and Schroeder (1960) compared observed seasonal changes of heat content in the upper 200 meters of the North Atlantic with estimates of surface heat fluxes. For the March to August heating season, the rate of heat storage was found to exceed the seasonal change of the surface heat flux at all latitudes between 20°N and 50°N. This would imply that the heat storage in the upper layer is amplified by seasonal changes in horizontal heat advection or by exchange across the bottom of the upper ocean layer, that is, the right hand side of (14b).

Fofonoff and Tabata (1966) analyzed observations in the North Pacific and showed the seasonal variation of sea surface temperature to be primarily determined by the heat flux at the surface. Variations of isopycnal depths were apparently related to the wind stress curl in accordance with (10) and (13) but observed movements were up to ten times larger than calculated from observed winds. Near the coast, vertical movements appeared related to Ekman transports normal to the coast.

Bathen (1971) compared rates of heat storage in the upper 250 meters of the North Pacific with seasonal variations of surface heat flux. He retained only nondivergent advection and horizontal diffusion on the right of the heat balance equation (11a), thus implying that the Ekman terms (11b) are balanced by the vertical diffusion in (11c). Given monthly values of surface heat fluxes, he integrated

the heat conservation equation over an annual cycle for assumed circulation patterns. The process was repeated until satisfactory agreement was obtained between observed and computed heat storage over an annual cycle. His conclusion was that heat advection by nondivergent currents could be twice as large as the surface flux of heat.

Gill and Niiler (1973) have questioned Bathen's result noting that the rate of heat storage computed by the model does not balance the surface flux when integrated over an area enclosed by a streamline. They argue that an approximate local balance is maintained between the rate of heat storage and seasonal variations of surface heat flux, that is, the right hand side of (14b) tends to vanish. They eliminated nondivergent advection by recourse to a scale analysis and computed seasonal changes of horizontal and vertical heat advection by Ekman currents for the upper 200 m of the North Pacific and North Atlantic and found them to be an order of magnitude smaller than observed rates of heat storage. They did not attempt to balance the terms of equation (14b) for the whole oceans but they did find satisfactory local balance at weather ship stations and hence blamed the data for any imbalances at larger space scales.

The computation of Ekman transports, in particular, has received a great deal of interest in the past. Fofonoff (1962) discusses computer programs for routine calculation of Ekman currents as well as geostrophic currents for specified surface winds over the ocean. Gill and Niiler (1973) and others computed Ekman pumping from Hellerman's (1967) wind stress data for the world oceans. Recently, Leetmaa and Bunker (1978) calculated Ekman transports from Bunker's (1976) wind stress estimates for the North Atlantic. Meyers (1975) computed seasonal variations of Ekman pumping in the trade wind zone of the North Pacific and found that the observed deepening of the 20°C isotherm during spring could be explained by strengthening of the curl of the

wind. White (1977; 1978) emphasized that changes in depth of the thermocline are not just determined by local winds, but that there is an additional response propagating from the eastern boundary in the form of baroclinic Rossby waves. Schopf (1980), however, found the process of Ekman pumping and Ekman drift able to account for observed seasonal variations of heat transport across the equator. The addition of wave phenomena within the framework of a bounded ocean model did not seem to alter the net cross-equatorial flow.

A number of studies have been devoted to the closely related problem of anomalies in sea surface temperatures. The assumption is then that the anomalies are governed by equations similar to (14b) and (15) where the primes denote deviations from the normal seasonal cycle. Namias (1965) used anomalous Ekman currents to advect normal sea surface isotherms in the North Pacific, ignoring effects of upwelling or downwelling. In a subsequent paper, Namias (1972) related SST-anomalies to anomalous surface heat fluxes and to horizontal advection by normal currents. Jacob (1967) also considered advection of normal isotherms by anomalous currents as well as advection of anomalous isotherms by normal currents and effects of anomalous heating. These studies seem inconclusive as to the relative importance of the various contributions.

White et al. (1980) found the thermocline in the mid-latitude North Pacific to respond to anomalous atmospheric forcing as expected from Ekman pumping theory during most of the year. However, during late autumn, the response of the thermocline appeared to be opposite to the direction of the Ekman pumping. Haney (1980) investigated the sensitivity of a 10-level Pacific Ocean model to anomalies in prescribed wind stress and surface heat flux and found qualitative agreement with observed anomaly development during the fall of 1976.

3 HEAT BALANCE COMPUTATIONS

The various terms in the heat balance equations (14a-b) have been computed from climatological data for the northern hemisphere oceans. The calculations were carried out on a grid of 10° latitude by 10° longitude and the results were averaged zonally over all oceans and for the Atlantic and Pacific separately. To obtain seasonal values, data were used for January, April, July and October, respectively, and annual means were defined as averages of these four seasonal values.

Oceanic Heat Storage

Oceanic temperatures and rates of heat storage in the ocean were obtained from the Bauer-Robinson (1977) numerical atlas. The atlas contains temperatures for every 1° quadrangle in the northern hemisphere oceans from the eqator to 65°N in the Pacific and to 73°N in the Atlantic. For each month, temperature values are presented in the seasonal layer at 30-m intervals down to 150 m and at NODC hydrocast levels below. For purposes of computing monthly values of heat content, temperatures were interpolated linearly between data levels. Monthly rates of heat storage were then obtained by subtracting heat contents for the preceding month from those for the following month. Hence, they refer to the middle of each month.

Distributions of rates of heat storage in the upper ocean for January and July are presented in the upper parts of Figs. 1a and 1b, respectively. The contour interval is 100 cal/cm^2/day and negative values are indicated by dashed lines. Zonal averages for each of the four seasons are depicted in Fig. 2. The individual points represent averages over the oceanic portion of a 10° latitude belt and they have been connected by solid lines for improved visualization. The points

connected by dashes in the same figure indicate corresponding results from Oort and Vonder Haar (1975). These authors state that their results are quite similar to those obtained from Bauer-Robinson, but it is seen that the differences are not inconsiderable. The present results show a distinctly larger seasonal amplitude, in particular when the greater depth of Oort and Vonder Haar's seasonal layer (275 m) is taken into consideration. An exact analysis of the differences is not possible because the data base of Oort and Vonder Haar is not yet publicly available.

Surface Heat Flux

Climatological values of total heat balance at the ocean surface were obtained from Budyko's atlas as presented by Schutz and Gates (1971; 1972; 1973; 1974). The heat balance data represent net downward radiation flux at the sea surface minus upward flux of sensible and latent heat. The data are available on a global grid of 4° latitude by 5° longitude for the months of January, April, July and October. All land values were eliminated before obtaining averages over 10° quadrangles to prevent contamination of values in nearshore grid points by land values. The resulting distributions of downward surface flux over the northern hemisphere oceans are shown at the bottom of Figs. 1a and 1b for January and July, respectively. In January there is a good correlation between patterns of heat storage and surface flux with large heat losses occurring along western ocean boundaries as a result of cold air flowing over relatively warm water. In July the pattern shows a similar correlation but the magnitude of the heat storage substantially exceeds that of the surface flux. At low latitudes in the eastern parts of the oceans, irregular distributions of heat storage are found which are not reflected in the surface

flux. Such changes in heat storage are apparently related to other processes such as horizontal and vertical circulations.

Zonal averages of surface heat fluxes for each of the four seasons are presented at the bottom of Fig. 2 where averages refer again to the land portion of each zonal belt and individual points are connected by solid lines. For comparison, points connected by dashes indicate the corresponding values derived by Oort and Vonder Haar (1976) from considerations of the atmospheric energy budget. In the latter, the surface flux appears as an imbalance between observed radiation flux at the top of the atmosphere and rate of storage and divergence of transports of atmospheric energy. It is assumed that the land has no heat capacity and that the residual surface flux obtained from the atmospheric energy balance is completely stored in the ocean. For a discussion of the discrepancies between the two sets of averages, the reader is referred to Oort and Vonder Haar (1975).

Recently, new estimates of heat fluxes over the oceans have been obtained on the basis of ship weather observations. For the Atlantic, monthly means for all months from January, 1948 through December, 1972 are available on data tapes from the Woods Hole Oceanographic Institution (Bunker and Goldsmith, 1979). Comparison with Budyko's estimates (Bunker, 1976; Bunker and Worthington, 1976) indicates that the overall distribution patterns are similar. The major change is an annual mean warming of nearshore waters from Nova Scotia down to Cape Hatteras instead of the strong cooling over the continental shelf in Budyko's estimates. Similar calculations have apparently been performed for the Pacific by N. Clark of the Scripps Institute of Oceanography, but the results were not available at the time of the present study.

Heat Transport by Ekman Drift

Effects of Ekman currents on the heat balance of the upper ocean layer have been discussed in connection with (12). The effects essentially consist of convergence of horizontal heat transports in the surface layer plus vertical heat transport through the bottom of the layer due to Ekman pumping. The horizontal components of the Ekman drift are obtained from the surface wind stress in accordance with (13) whereupon the vertical Ekman pumping follows from (10). The present calculations are based on climatological values of surface stress over the world oceans presented by Hellerman (1967). The data are available on a grid of 5° latitude by 5° longitude for each of the four seasons. Seasonal surface temperatures were taken from the Bauer-Robinson (1977) numerical atlas. The bottom temperature was taken to be the annual mean temperature at the 250 m level.

The Ekman heat transports (11b) were calculated on a 10° by 10° grid with a staggered distribution of variables. Horizontal water transports were defined at the sides of each quadrangle and temperature and vertical motion at the centre. Horizontal heat transports across the sides of grid squares were obtained by averaging temperatures of two adjacent squares. The relationship (13) between the Ekman drift and the wind stress can only be used in the open ocean. On the lateral boundaries of the oceans the normal component of the horizontal Ekman transport must vanish. If this is used as a boundary condition and the continuity equation (10) is applied to all grid squares, upwelling will result for Ekman drift away from the coast and downwelling for onshore flow. The result does not reflect the dynamics of coastal regions and as such it is not meaningful. However, it does satisfy conditions of mass balance and the effect is often more clearly visible in observational data than the effect of the wind curl in the open ocean (see, e.g., Fofonoff and Tabata, 1966). Thus, the

Ekman pumping and the associated vertical heat transport are here computed for all grid points.

Near the equator, the Ekman relation (13) also breaks down. In order to estimate the Ekman transports there, the wind stress is separated into an annual mean component and the seasonal deviations from the mean. The zonal component of the annual mean stress is taken to be symmetric around the equator. The corresponding meridional component of the Ekman transport is antisymmetric and hence goes to zero at the equator. The corresponding vertical velocity in the latitude belt adjacent to the equator follows then from (10). The seasonal component of the stress is taken to be antisymmetric around the equator as discussed by Schopf (1980) and it is assumed to increase linearly with latitude. The corresponding meridional Ekman transport is constant and the seasonal vertical velocity component near the equator must vanish according to (10). Like the corresponding calculation for the nearshore zones, this procedure only satisfies conditions of mass conservation but it does not take into account the dynamics of the equatorial region (White, 1977; Schopf, 1980).

Annual Heat Balance

The individual components of the heat balance (11) are discussed for the annual mean and the seasonal deviations, separately. The annual mean distribution of convergence of heat transport in the upper ocean is shown in the upper part of Fig. 3a. As defined under (11), this convergence of heat is obtained as the difference between the local rate of heat storage and the local surface flux of heat. In the annual mean, therefore, the convergence of heat equals the upward heat flux at the sea surface. The left side of Fig. 4 shows the annual downward surface heat flux averaged zonally over all oceans (top) and

for the Atlantic (middle) and Pacific (bottom) separately. At high latitudes there is an upward surface flux and convergence of heat transport; at low latitudes a downward flux and divergence of transport. Integration of heat convergence southward from the North Pole gives oceanic heat transport across given latitudes (but not necessarily in the upper layer). Thus, the ocean transports heat from low latitudes to high latitudes. As noted in the Introduction, the ocean model should reproduce this result in the annual mean.

The annual mean distribution of the total Ekman effect (11b) is presented in the lower half of Fig. 31. The values are seen to increase strongly toward the equator but the results naturally depend on the depth of the Ekman pumping, here assumed to be 250 m. In the belt adjacent to the equator,upwelling and cooling are caused by the northward Ekman drift across 10°N. This is also a typical result of three-dimensional ocean models (e.g., Bryan et al., 1975) but then this vertical circulation cell is much shallower than assumed here. In view of the uncertainty surrounding the results of Ekman calculations near the equator, these values have not been entered in the map of Fig. 3a, but, as a matter of interest, they are indicated by the dash-dot lines in the zonal averages of Fig. 4.

The heat advection by Ekman currents is subtracted from the convergence of total heat transport to obtain the residual term in the heat balance (11c), the annual average of which is presented in the upper half of Fig. 3b. As defined by (11c), this term includes horizontal advection of heat by large scale inviscid (generally quasi-geostrophic) currents which, as discussed under (9), may in first approximation be considered non-divergent and hence may be represented by a streamfunction. An estimate of the latter effect can be obtained by combining the Bauer-Robinson (1977) upper ocean temperatures with

available estimates of large scale ocean circulations. By way of example, a calculation has been made for the North Pacific using the streamfunction estimated by Bathen (1971). No adjustments were made for any Ekman transports included in this circulation. The streamfunction is essentially zero at 10°N such that the heat in the basin is only redistributed but the integrated heat change must vanish. The result averaged over all seasons is shown at the bottom of Fig. 3a and averages for 10° latitude belts in the Pacific are illustrated by the dashes in Fig. 4.

Seasonal Heat Balance

Seasonal deviations from the annual mean convergence of heat transports in the upper ocean are presented in the upper half of Figs. 5a and 5b for January and July, respectively. As before, this heat convergence is derived by subtracting the local downward surface flux of heat from the local rate of heat storage (Figs. 1a and 1b) and subtracting the annual mean based on the four seasonal values. The results show irregular patterns, representing in many cases relatively small differences between large numbers or slight phase shifts between similar patterns of heat storage and surface flux. The results are, therefore, more likely a measure of observational error than of physical processes. Zonal averages for all oceans and for the Atlantic and Pacific separately are presented in Figs. 6a and 6b.

Seasonal deviations from the annual mean convergence of heat by Ekman transports are shown in the lower parts of Figs. 5a and 5b and the corresponding zonal averages are included in Figs. 6a and 6b. These values were obtained by computing the total heat convergence in the surface layer due to horizontal Ekman transports and vertical Ekman pumping for each season and then subtracting the annual mean

shown in Fig. 3a. Near the equator the results become unreliable and therefore they have not been included in the maps. It was mentioned before that the seasonal component of Ekman pumping tends to vanish in this region. This is indicated by the dash-dot lines in Figs. 6a and 6b. It should be added, though, that actual computations of the seasonal Ekman effect from the curl of the wind at the centre of this belt (5°N) does not produce small values but in general shows positive deviations in January and negative values in July.

The July results for the Atlantic (Fig. 6b) and similar results for April (not shown) confirm the conclusion of Bryan and Schroeder (1960) that the surface heat flux during the heating season would be augmented by heat advection if these results were true. Seasonal variations of heat advection by non-divergent circulations were estimated from Bathen's annual mean streamfunction and seasonally varying temperatures for the Pacific. The seasonal deviations from the annual mean were found to be small in agreement with the scale analysis of Gill and Niiler (1973). The results could, however, be different if the large scale circulation were allowed to vary from season to season.

As seen from (15), the seasonal component of the Ekman effect consists of advection of annual mean temperatures by seasonal Ekman currents plus advection of seasonal temperatures by mean Ekman currents. These individual contributions are ilustrated in Fig. 7. The total Ekman effect is presented at the top, the terms within the first pair of square brackets in (15) are displayed in the middle, and the terms within the second pair of brackets are shown at the bottom of Fig. 7. The last term on the right of (15) is found to be negligible. The other terms appear somewhat comparable in magnitude, not unlike the conclusions reached in studies of SST anomalies (Namias, 1965; 1972; Jacob, 1967).

4 STRATIFICATION MODEL

An essential element of upper ocean models is the mechanism of mixed-layer formation due to the interaction between wind-induced mechanical turbulence and stability effects resulting from surface heating. A second mechanism is the formation of a deep mixed layer due to convective overturning in the presence of surface cooling. These processes are in essence locally determined and have been successfully simulated by one-dimensional models. These models can be divided into two main classes: mixed-layer models and turbulence closure models.

Mixed-layer models were introduced by Kraus and Turner (1967) and have been reviewed by Niiler and Kraus (1977). An upper ocean layer with uniform temperature is postulated and the depth and temperature of the layer are estimated from energy considerations. Models of this type have been used to simulate observed annual temperature cycles at weather stations in the Atlantic (Gill and Turner, 1976) and the Pacific (Thompson, 1976; Haney and Davies, 1976). These and other generalizations of the Kraus-Turner model (Kim, 1976; Garwood, 1977) appear to reproduce the major properties of the upper ocean temperature structure on an annual basis. Wells (1979) coupled this kind of model to an atmospheric general circulation model of the southern hemisphere, taking into account advection of temperature and salinity by Ekman drift. Kim and Gates (1979) embedded Kim's (1976) model into a four-layer general circulation model of the world ocean.

Turbulent closure models are based on the conservation equations for heat and momentum in the Reynolds-averaged form with turbulent fluxes formulated in terms of mean variables and higher moments of fluctuations. These formulations may be approximated in various ways and in the simplest type of equilibrium closure the turbulent fluxes

become proportional to gradients of mean quantities (Mellor and Durbin, 1975; Kundu, 1980). The eddy coefficients involved are functions of stability and turbulent kinetic energy and they may be determined empirically (Munk and Anderson, 1948) or to some extent be derived (Mellor and Yamada, 1974). The maximum simplification of this type of model is achieved by prescribing the vertical current shear as a function of surface conditions instead of solving the momentum equations (Sundaram and Rehm, 1973; Walters et al., 1978).

The present study utilizes a model of the last type without explicit solution of the momentum equations. The model is based on the turbulent closure model of Mellor and Durbin (1975) but the vertical shear of the current is obtained from a solution of the steady-state equations of motion. This approximation was found to lead to a substantial increase in robustness of the model without any reduction of the quality of simulations of seasonal temperatures in Lake Ontario (Simons, 1980). A brief description of the model and its verification will be presented here.

Model Equations

The model is based on the one-dimensional temperature conservation equation:

$$\frac{\partial \overline{T}}{\partial t} = \frac{1}{\rho c_p} \frac{\partial \overline{I}}{\partial z} + \frac{\partial}{\partial z} \left(\overline{-w'T'} \right) \qquad (16)$$

where t is time, z is the upward vertical coordinate, T is temperature, ρ is density, c_p is specific heat, I is radiation, w is vertical velocity, the bars denote mean quantities and the primes denote

turbulent fluctuations. The turbulent flux equations may be simplified by recourse to the Kolmogoroff and Rotta hypotheses for the dissipation and pressure fluctuation terms and by neglecting the time variations as well as the triple correlations (Mellor and Yamada, 1974). The result may be expressed in the form:

$$\overline{-w'T'} = K \frac{\partial \overline{T}}{\partial z} \tag{17}$$

where the eddy diffusivity, K, is a function of the mixing length, the turbulent kinetic energy, and the stability as determined by the Richardson number

$$Ri = \alpha g \frac{\partial \overline{T}}{\partial z} \left| \frac{\partial \mathbf{v}}{\partial z} \right|^{-2} \qquad \alpha \equiv -\frac{1}{\rho} \frac{\partial \rho}{\partial T} \tag{18}$$

where g is the earth's acceleration and $\mathbf{v}$ is the horizontal current.

For the stable case ($Ri > 0$) it may be shown (Simons, 1980) that the diffusion coefficient is approximately given by:

$$K = (1 - 4\ Ri)^{3/2}\ \ell^2 \left| \frac{\partial \overline{w}}{\partial z} \right| \tag{19}$$

where ℓ is a mixing length, assumed constant. For $Ri > .25$ turbulent mixing is suppressed ($K = 0$). For unstable conditions ($Ri < 0$) satisfactory results are obtained by augmenting the eddy diffusivity by an amount

$$K' = \gamma \left(-\alpha g \frac{\partial \overline{T}}{\partial z}\right) \tag{20}$$

where the value of γ determines the rate of adjustment from unstable to neutral conditions.

In a complete turbulent closure model the current shear entering in (18) and (19) is obtained by solving the time dependent form of the equation of motion for the horizontal current. For the time scales of interest here it was shown by Simons (1980) that essentially the same results are obtained by a simpler procedure based on the steady-state equation of motion

$$fw \times \hat{k} + \frac{\partial}{\partial z}(\overline{-w'w'}) = 0 \qquad (21)$$

where f is the Coriolis parameter, $\hat{k}$ is the vertical unit vector, and the turbulent flux term takes the form

$$\overline{-w'w'} = A \frac{\partial \bar{w}}{\partial z} \qquad (22)$$

The functional variation of the eddy viscosity A is similar to (19).

To solve this system, consider the nearly homogeneous layer between the surface nd the thermocline were the eddy viscosity may be approximated by the neutral value

$$A = \ell^2 \left|\frac{\partial \bar{w}}{\partial z}\right| \qquad (23)$$

From (22) and (23) and the boundary conditions at the free surface it follows that:

$$\left|\frac{\partial \bar{w}}{\partial z}\right|_0 = \frac{\tau_0}{\rho A_0} \qquad A_0 = \ell\sqrt{\frac{\tau_0}{\rho}} \qquad (24)$$

where τ represents the magnitude of the stress vector and the subscript 0 denotes surface values. The problem posed by (21) to (24)

has been solved by Ekman (1905) and the solution for the current shear may be written as follows:

$$\left|\frac{\partial \bar{v}}{\partial z}\right| = \left|\frac{\partial \bar{v}}{\partial z}\right|_0 \left(1 + \frac{z}{D}\right)^2 \qquad D = 5\sqrt{\frac{A_0}{f}} \tag{25}$$

The vertical variation of the eddy viscosity is the same as that of the current shear in accordance with (23).

The unknown parameter of the model is the mixing length, ℓ. Following Mellor and Durbin (1975) it is assumed that the length scale is proportional to the ratio of the first to the zeroth moment of the turbulence field

$$\ell = \delta \int_{-\infty}^{0} |z| \left|\frac{\partial \bar{v}}{\partial z}\right| dz \Big/ \int_{-\infty}^{0} \left|\frac{\partial \bar{v}}{\partial z}\right| dz = \frac{5}{4}\,\delta\sqrt{\frac{A_0}{f}} \tag{26}$$

where use has been made of (25) and where the proportionality factor should be of order $\delta \approx 0.1$. Combining this result with (24) gives:

$$A_0 = \frac{\varepsilon \tau_0}{f\rho} \qquad \varepsilon \equiv \frac{25}{16}\,\delta^2 \approx 0.01 \tag{27}$$

The expression for the neutral current shear (25) is now used to approximate the Richardson number (18). With recourse to (24) and (27) the result is:

$$Ri = \left(\frac{\varepsilon}{f}\right)^2 \alpha g \frac{\partial \bar{T}}{\partial z}\left(1 + \frac{z}{D}\right)^{-4} \tag{28}$$

The neutral value of the eddy diffusivity, K, is approximated by the value of the eddy viscosity corresponding to (23), (25) and (27) and the result is adjusted for stability according to (19)

$$K = \frac{\varepsilon \tau_0}{f\rho} (1 - 4\ Ri)^{3/2} \left(1 + \frac{z}{D}\right)^2 \qquad (29)$$

For numerical calculations it is advantageous if the shear varies more gradually with depth for $z \approx -D$ than implied by (25). For depths of order $\sqrt{A_0/f}$ this solution can be quite well approximated by:

$$\left|\frac{\partial \bar{w}}{\partial z}\right| = \left|\frac{\partial \bar{w}}{\partial z}\right|_0 e^{z/\Delta} \qquad \Delta = 2\sqrt{\frac{A_0}{f}} \qquad (30)$$

The corresponding expression for (28) is:

$$Ri = \left(\frac{\varepsilon}{f}\right)^2 \alpha g \frac{\partial \bar{T}}{\partial z} e^{-2z/\Delta} \qquad (31)$$

The vertical variation of the eddy viscosity is the same as that of the shear (30) and the stability effect in (29) may be generalized to:

$$K = \frac{\varepsilon \tau_0}{f\rho} (1 + \sigma Ri)^{-1} e^{z/\Delta} \qquad (32)$$

where the coefficient σ should be of order $\sigma \approx 4$ which is in reasonable agreement with various empirical determinations (Karelse et al., 1974).

It is seen that in this model the wind-induced turbulence at all depths is related directly to surface conditions through a Richardson

number. The explicit solution of the momentum equation (21) is replaced by a functional relationship between vertical current profile and surface wind stress. This effectively uncouples the temperature and current structures but the essential interaction between wind and stratification is retained. A similar argument was used by Sundaram and Rehm (1973).

At the sea surface, the vertical flux of heat must be prescribed. The total heat flux at the surface, Q_s, is the balance of shortwave and longwave radiation plus sensible and latent heat. All of this is absorbed by the upper few meters of the ocean except about one-third of the incoming solar radiation which may be represented by an exponential decay formula. Since the penetrating part of the shortwave radiation is already accounted for by the first term on the right of (16), the boundary condition is:

$$-(\overline{w'T'})_0 = \frac{Q_s - I_s}{\rho c_p} \tag{33}$$

Model Tests

Figure 8 shows results of this model as applied to the same initial temperature profile used by Mellor and Durbin (1975). The left hand diagram shows the thermocline variation as a function of the inertial period $P=2\pi/f$ for a steady wind stress $\tau_0=2$ dynes/cm^2. The values of the model parameters are $f=10^{-4}$ s^{-1}, $\alpha g=0.173$ cm s^{-2} K^{-1}, $\varepsilon=0.01$ and $\sigma=4.0$. The solid lines in the middle diagram show the corresponding profiles of the eddy diffusivity, K, and the dashed line represents the neutral value of K. The right hand diagram compares results after 10 inertial periods for different values of the wind stress and the stability parameter σ. The effect of this parameter is

as expected. On the other hand, the model is found to be relatively insensitive to variations in the parameter ε by a factor two or so because its effect on the neutral value of K tends to be compensated by its effect on the Richardson number.

In order to verify the model, data were used from the 1972 International Field Year for the Great Lakes. As part of this data base, three-dimensional temperature distributions and heat budgets for Lake Ontario are available at weekly intervals (Canada Centre for Inland Waters, 1979). The data were averaged horizontally over the whole lake to obtain a seasonal stratification cycle for space scales of interest in the present study. Calculations started on April 1, 1972, with a homogeneous temperature of 2°C and continued for one year.

Initial experiments utilized the complete Mellor-Durbin (1975) model with a vertical structure of 75 layers of 2-m thickness and a time step of one day. The model has one adjustable parameter, viz., the coefficient δ appearing in (26), which was set equal to $\delta=0.2$ as suggested by the original authors. As shown by Simons (1980) this value yields quite satisfactory agreement with the Lake Ontario observations. However, the convergence of the iteration procedure required for numerical solution of the model equations was found to be poor. A closely related problem is that substantial variations of solutions may be found for small changes of input parameters which are well within the error margin of the data. The model, therefore, was not considered to be a reliable and efficient computing device to model the upper ocean as part of a large scale circulation model.

The simplified model based on equations (16), (17), (20), (31), and (32) has three coefficients, viz., γ, ε, and σ. The first one is determined by requiring full mixing to occur under unstable conditions which appears to be accomplished if γ exceeds the value 10^7 cm^2 s.

The second coefficient corresponds to the parameter δ of the Mellor-Durbin model by virtue of (27). It is assigned a value ε=0.01 as in the experiments of Fig. 1, but, as noted above, the model is rather insensitive to this parameter. The third coefficient, σ, should be of order $\sigma \approx 4$, but it appears necessary to reduce this to σ=2 for better agreement with observations. The corresponding results obtained from the Lake Ontario simulations are shown in Fig. 9.

While the simplified model has the drawback of a somewhat arbitrary stability parameter, σ, it has considerable numerical advantages. The equations of motion are not solved and, furthermore, the solution turns out to be quite independent of the number of iterations, a single iteration being sufficient. The model, therefore, appears suitable for the present purpose.

5 UPPER OCEAN SIMULATIONS

The stratification model presented above is now modified to include the advective contributions to the heat balance of the upper ocean discussed in the first part of this report. The basic equation is the heat conservation equation (1) combined with the continuity equation (2) and with the vertical component of the diffusive heat flux formulated according to (17)

$$\frac{\partial T}{\partial t} = \frac{\partial}{\partial z}\left(K \frac{\partial T}{\partial z}\right) - w \frac{\partial T}{\partial z} - \mathbf{v}\cdot\nabla T + \nabla\cdot\mathbf{\Gamma} \qquad (34)$$

where K is given by (32) for stable stratification and by (20) for unstable configurations. As noted under (7), the vertical velocity in the upper ocean is due mostly to the Ekman pumping, w_e, whereas the horizontal current may be written as the sum of an inviscid component

$\mathbf{v}_i$ and the Ekman drift $\mathbf{v}_e$. The temperature equation may then be written as follows:

$$\frac{\partial T}{\partial t} = \frac{\partial}{\partial z}\left(K \frac{\partial T}{\partial z}\right) + e + r \tag{35a}$$

$$e = -w_e \frac{\partial T}{\partial z} - \mathbf{v}_e \cdot \nabla T \tag{35b}$$

$$r = -\mathbf{v}_i \cdot \nabla T + \nabla \cdot \Gamma \tag{35c}$$

Vertical integration of (35a) with boundary condition (33) results, of course, into the heat balance equation (11a) with

$$E = \int_{-h}^{0} e\,dz; \qquad R = \int_{-h}^{0} r\,dz - Q_h \tag{36}$$

where Q_h is the downward heat flux at the bottom of the upper ocean layer.

Although heat balance equations can be written down for the annual mean and the seasonal components separately as done in (14a-b), this type of separation is not practical for (35a-c) in view of the nonlinear coupling terms. For subsequent analysis of model results it is, however, instructive to express the equation and the surface boundary condition in terms of annual mean and seasonal contributions to temperature variations. Denoting these components again by bars and primes, respectively, one obtains:

$$\frac{\partial T}{\partial t} = \frac{\partial}{\partial t}\left(K \frac{\partial T}{\partial z}\right) + (\bar{e} + e') + (\bar{r} + r') \tag{37}$$

$$K \frac{\partial T}{\partial z}\Big|_0 = \frac{\bar{Q}_s + Q_s'}{\rho c_p} \tag{38}$$

In the usual oceanic application, (37) is solved without regard to any advective effects (e=r=0) and without the annual mean component of the surface heat flux, that is, with boundary conditions

$$K \frac{\partial T}{\partial z}\Big|_0 = \frac{Q_s'}{\rho c_p} \tag{39}$$

Long-term effects of such a surface heat flux with zero running mean over an annual cycle have, for instance, been analyzed in great detail by Wetherald and Manabe (1972). For purposes of climatic simulations, however, this boundary condition must be rejected in view of the established fact that the ocean extracts heat from the atmosphere at low latitudes and returns it at high latitudes. It follows that, if a model were calibrated by using the boundary condition (39), it would underpredict sea surface temperatures at higher latitudes under actual conditions as expressed by (38). Adding the solution to (37) subject to the annual mean surface heat flux, would not alter the result because the locally upward surface flux is presumably compensated by advective and diffusive processes such that the left hand side of (37) is zero in the annual mean. Consequently, (37) must be solved subject to the complete boundary condition (38) and the solution cannot be obtained by solving (37-38) for the annual mean and seasonal components separately and then adding the results.

Method of Calculation

The temperature prediction equation (37) is solved at 75 levels below the surface with uniform vertical spacing of 3 m. An implicit time extrapolation scheme with a time step of one day, an iterative procedure for obtaining the diffusion coefficient, K, and a matrix inversion for solving the system of finite difference equation in the

vertical are used. The model parameters are assigned values similar to those used in the Lake Ontario simulations mentioned above. The thermal expansion coefficient defined by (18) is approximated by recourse to climatological salinity data from the Bauer-Robinson (1977) numerical atlas. For this purpose, the density is represented as a quadratic function of temperature with coefficients determined from local salinity data in accordance with the approximate equation of state of Friedrich and Levitus (1972) and Bryan and Cox (1972). The thermal expansion coefficient then enters into the model as a linear function of temperature with space-dependent coefficients.

Model forcing, as well as initial and boundary conditions, are obtained from the same data base used for the heat balance computations presented above. As noted in that context, heat balance components (11a-c) were computed for January, April, July and October. For simplicity, a linear time interpolation was used for the Ekman effect (11b) and the residual term (11c). Since the rate of heat storage is available from the Bauer-Robinson atlas for every month, monthly values of the surface heat flux are obtained by subtracting the linearly interpolated values of the right hand side of (11a) from the monthly rates of heat storage. It should be noted here that the "observed" Ekman effect (11b) is used only for this computation and interpolation of the residual term, R, and the surface heat flux, Q_s. The Ekman effect enters into the model in accordance with (35b) and hence it is determined by wind-driven Ekman currents in conjunction with temperatures predicted by the model. Only for a perfect model, the two effects would be the same.

In contrast to the Ekman effect, e, the residual term, r, in (35a) is not recomputed from predicted temperatures because the corresponding circulation patterns and effective diffusion coefficients are not considered sufficiently well known. The question then arises

how the "observed" residual term, R, is to be distributed in the vertical. In as much as this term is due to horizontal advection and diffusion, a reasonable first approximation would be to assume a uniform distribution throughout the surface layer, hence from (36)

$$r = (R + Q_h)/h \tag{40}$$

where h is the depth of the layer. After some experimentation with more sophisticated vertical distributions as a function of temperature profiles, it was concluded that (40) was an acceptable approximation. Note that in view of our sign convention for the vertical diffusion (positive downward) it appears from (40) as if the vertical heat flux at the lower boundary is added to the residual term R and then distributed uniformly over depth. In actual fact, the term R includes the bottom flux according to (36) and thus the latter is subtracted in (40) such that only the difference is distributed over depth.

Since the temperature at the bottom of the model layer is better known than the heat flux, the logical boundary condition would be to prescribe the temperature. The heat flux would then be computed by the model. However, the turbulence model is designed to simulate stratification effects near the surface but does not render meaningful information on any diffusive processes that may be operating at greater depths. As a matter of fact, diffusion coefficients computed from this type of model will always be negligibly small at the bottom of the model layer unless the density profile is unstable. For stable situations, then, prescribing the bottom temperature is equivalent to prescribing zero heat flux. For unstable conditions, on the other hand, prescribing the bottom temperature allows for unlimited heat supply in certain situations, for instance when the residual term (35c) is negative. This is undesirable since the present model is intentionally constrained by principles of heat conservation. After

some experimentation it was therefore decided to use the zero flux condition at the lower boundary. Its effect on the sea surface temperature is in any case much smaller than its effect on the heat balance of the whole layer.

The Ekman currents entering into (35b) are computed by recourse to linearly interpolated seasonal wind stress data as published by Hellerman (1967). The vertical distribution of the horizontal current may be obtained from the complete Ekman solution corresponding to (25) if the vertical distribution of the eddy viscosity is assumed to be similar to that of the eddy diffusivity. The vertical Ekman pumping as a function of depth follows then from (2). Below the Ekman layer the frictionally induced vertical velocity will remain constant while in the mixed layer its variation is irrelevant because the temperature gradient vanishes. As long as the Ekman depth is not much greater than the mixed layer depth, it is therefore permissible to treat the Ekman pumping as a constant in (35b). The horizontal advection in (35b) is, in the present model, the only term effecting a horizontal coupling of the various grid points. It would seem inconsistent to compute this term in great detail while approximating the remaining horizontal coupling terms (35c) in such a crude fashion. An approximation like the first term on the right of (12) should be acceptable. Furthermore, while Fig. 7 shows that the horizontal Ekman advection is comparable to the vertical advection for the seasonal component, it turns out that both effects are very small. The annual mean component of the Ekman effect, on the other hand, is large at low latitudes but this effect is almost totally due to vertical advection. In view of this, it was found convenient to limit explicit calculation of the Ekman effect to the vertical advection only. The residual term r appearing in (35a) was redefined to include the horizontal Ekman advection and the corresponding term R in (11a) was recomputed accordingly.

The Hellerman wind stress data are equivalent to vector-averages in time and, as such, they should be adequate for estimating Ekman pumping. By contrast, the turbulence model (32) is affected by the absolute value of the wind stress and hence the forcing must include oscillatory components of the stress such as effects of storms and other transient meteorological phenomena which are eliminated by vector-averaging. In a study of a somewhat analogous problem, Fissel et al. (1977) found that near 50°N the stress computed from monthly averaged winds was typically half as large as the monthly average of daily stress values. This ratio naturally varies strongly with latitude. In particular, in the mid-latitude transition zone between mean easterlies and mean westerlies, the vector-averaged stress is negligible by comparison to the scalar average, whereas at low latitudes the winds are so steady that the two averages are nearly equal. For the present calculations, therefore, monthly averages of the magnitude of the stress were computed from the U.S. Marine Climatic Atlas of the World as revised in 1974 for the North Atlantic and in 1977 for the North Pacific. The atlas presents, for selected locations, wind frequencies for eight directions and ten speed classes. For each class, the stress was computed using the same stress coefficients adopted by Hellerman (1967) and the scalar averages of all results for a given month and location were compared with the vector-averages. Latitudinal variations of seasonal values are shown in Fig. 10 for the North Atlantic near 40°W and the North Pacific near 170°W. Monthly means of the magnitude of the stress are shown by the solid curves; vector-averaged stresses are denoted by dash-dots, and the corresponding values computed by Hellerman are shown by dashes. The differences between the latter two results are probably due to differences in the data base and methods of interpolation. It may be added that it is also possible to compute monthly averages on the basis of the rate of production of turbulent energy, $\tau^{3/2}$, but this does not lead to such large differences.

Results of Simulations

The upper ocean model presented above was applied to the northern hemisphere oceans on a grid of 10° latitude by 10° longitude. All simulations started in the middle of the month of April. Initial vertical temperature profiles were obtained from the Bauer-Robinson atlas by linear interpolation between the seasonal temperatures at the six available levels in the surface layer and the annual temperature at the lower boundary of the model (225 m). The overwhelming amount of results render it impossible to present a detailed description of model performance with regard to both time and space. Besides, it seemed more interesting to first gain insight in the contributions from individual components of the model toward the total solution. At the risk of losing possibly interesting spatial information, it was therefore decided to concentrate on selected latitudinal bands across the North Pacific and the North Atlantic and to perform a rather complete sensitivity analysis for those areas. The present discussion will be limited in that sense. Any systematic spatial deviations from the present patterns, if they exist, will be addressed when the model is coupled with the atmospheric GCM.

The latitudinal bands selected for discussion are 30 to 40°W in the Atlantic and 170 to 180°W in the Pacific. The wind stress components were shown already in Fig. 10. Seasonal variations of the individual components of the heat budgets (11a-c) for 10° latitudinal portions of these bands are shown in the left hand panels of Figs. 11 and 12, respectively. Corresponding variations of observed temperatures at three levels in the vertical are shown on the right. This data sample appears to include a rather complete range of conditions to be encountered in the world oceans. Of particular interest are the latitudinal variations of the relative contributions from individual components of the total heat budget and the latitudinal variations of

the vertical temperature structure. Specifically, as noted above, it is seen that the annual mean surface flux reverses its sign between high and low latitudes with a corresponding sign reversal of the residual advection re presented by R.

To facilitate comparison of results from various model experiments, it is convenient to select one of them as a bench mark and to consider all others in relation to this basic experiment. It will be seen that effects of individual modifications of the model are quite systematic in nature such that the result of combining a number of such modifications can be readily anticipated. The choice of the basic model is rather arbitrary but it is preferable that it be somewhere in between the most complete and the most truncated version of (37)-(38). It was decided, therefore, to choose the model version which is not affected by any annual mean components of heat fluxes or heat advection, i.e., $\bar{Q}_s=\bar{e}=\bar{r}=0$ in (37)-(38). The model parameters ε and σ defined in (27) and (32) are assigned the values $\varepsilon=0.01$ and $\sigma=1$ in this basic experiment. Sea surface temperatures simulated by this model are shown by the solid curves in the left hand panels of Figs. 13 and 14 for the Atlantic and Pacific, respectively. The results are to be compared with the solid curves in the right hand panels of Figs. 11 and 12, respectively. It is seen that in the Atlantic seasonal temperature variations tend to be overestimated at middle latitudes and underestimated at low latitudes. In the Pacific, seasonal variations appear to be underestimated at all latitudes.

The first series of experiments is concerned with the values of the model parameters. Results of two such experiments are included in the left hand panels of Figs. 13 and 14. In the first case, shown by dash-dots, the stability parameter σ is doubled to $\sigma=2$. This naturally increases the sea surface temperature at all latitudes but apparently the increase is most pronounced at mid-latitudes in the

Atlantic where the basic model did already overestimate the temperature. In the second case, shown by dashes, the Coriolis parameter entering into the turbulence model (31)-(32) is assigned a uniform value of $f = 10^{-4}$. This is, in effect, equivalent to assuming that the generation of turbulent energy is not governed by Ekman dynamics but by some other mechanism (see, e.g., Niiler and Kraus, 1977). The main effect of this modification is to increase the seasonal temperature cycle at low latitudes.

A second series of experiments concerns itself with the seasonal components of the Ekman effect, e', and the residual advection, r', in (37). Note that all annual components ($\bar{Q}_s$, $\bar{e}$, $\bar{r}$) are still zero. The results are shown in the middle panels of Figs. 13 and 14. The solid curves represent the case without Ekman heat advection. In this case, the residual forcing term, r', has been adjusted to maintain the heat balance (11a); in other words, the residual term now consists of the sum of (35b) and (35c) and it is specified a priori. For all practical purposes the results are identical to those from the basic experiment. The dashed curves in the middle panels are obtained if the residual term, r', is discarded. This is equivalent to neglecting the seasonal component of advection and placing greater confidence in the estimated surface heat fluxes than the observed rates of heat storage in the ocean. The dash-dots represent the opposite case where the residual term r' is added to the surface heat flux Q_s' such that the corrected heat flux equals the observed rate of heat storage. comparison of the results tends to favour the former supposition, at least at mid-latitudes.

A third set of experiments deals with the complete model including annual mean components of surface heat flux and advection. These results are shown in the right hand panels of Figs 13 and 14. The solid curves represent the case without explicit computation of Ekman

heat advection; this effect is included in the residual forcing term, r, which is computed a priori from the heat balance. As discussed above, the effect of including the annual mean component of the surface heat flux is to substantially reduce sea surface temperatures at higher latitudes. This is particularly true for the North Atlantic where, as seen from Fig. 11, there is a pronounced loss of heat from the ocean to the atmosphere at 45 to 55°N. It is discomforting, however, that inclusion of this term in the model does not lead to the anticipated improvement, but to considerable deterioration of results. No improvement is found if the Ekman effect is explicitly computed, that is, if the model is used in its complete form as formulated by (37)-(38). These results are shown by the dashed curves in the right hand panels of Figs. 13 and 14. It is seen that the sea surface temperature drops substantially at low latitudes where the annual mean Ekman effect supposedly makes a strong positive contribution to the heat budget as seen from Figs. 11 and 12. The reason for this inverse response of the present model is, of course, that this Ekman effect is counteracted by a large negative residual term, r, which affects the surface temperature more directly than the Ekman term as a result of approximation (40). It should be noted that this does not imply that the annual mean Ekman effect is erroneously included in the model; the fault lies probably with the lower boundary condition (Q_h=0) as well as the approximation (40).

A final experiment is shown by the dash-dots in the right hand panels of Figs. 13 and 14. This experiment was the same as the basic one but the diffusion coefficient was assigned a constant value of K=1.5 cm^2/s under stable conditions, as done by Wetherald and Manabe (1972). The solutions reflect seasonal variations of the surface heat flux shown in Figs. 11 and 12, but modified by overturning at times of unstable configurations. It would appear that it is worthwhile to include effects of wind mixing under stratified conditions, even if such

effects are as crudely approximated as done in the present turbulence closure model.

6 SUMMARY AND CONCLUSIONS

This report was concerned with the design and verification of an upper ocean stratification model suitable for coupling with an atmospheric general circulation model at seasonal time scales. The model is based on turbulence closure principles but it is drastically simplified to increase its efficiency and robustness without apparent loss of simulation capability. This aspect of the model was evaluated by recourse to detailed temperature observations and heat budgets available for Lake Ontario. Seasonal and annual heat budgets for the northern hemisphere oceans were computed to evaluate relative effects of turbulent heat fluxes, Ekman pumping, and large scale circulations on seasonal temperature variations in the upper ocean. The basic stratification model was then modified to incorporate advective effects on the basis of these heat budget calculations.

A series of model experiments were carried out to evaluate the sensitivity of the model to the turbulence closure parameters and to the annual mean and seasonal components of surface heating, Ekman pumping, and residual advective and diffusive effects. It was found that the Ekman dynamics inherent in the present turbulence closure approximation are not essential for adequate performance of the model. None of the model versions showed a systematic improvement of surface temperature predictions over those computed by the simplest model responding only to the seasonal component of surface heating and excluding all advective effects. Direct estimates of surface heat fluxes appeared to produce a more favourable model response than estimates based on local rates of heat storage in the ocean without regard

to seasonal variations of advection. Including the annual mean transport of heat by the ocean from low to high latitudes resulted in unexpected deterioration of model performance at high latitudes.

The present study was initiated with the purpose of embedding an upper ocean boundary layer model into a relatively coarse-resolution three-dimensional circulation model and this type of model was actually programmed at the start of this study for coupling with an atmospheric general circulation model. In light of the present analysis, however, it is now felt that this approach is not justified until it can be demonstrated that the large scale effects computed by this type of model are significantly greater than the uncertainties in other contributions to seasonal variations of sea surface temperatures addressed in this report. As such, the present study merely confirms the conclusions of Gill and Niiler (1973) and runs counter not only to our own initial approach, but also that of other recent studies in this field. It was decided, therefore, to couple the upper ocean model in its present simple form with the atmospheric general circulation model. That experiment will be described in a sequel to this report.

ACKNOWLEDGEMENTS

This work was partly carried out at the Canadian Climate Centre in Downsview, Ontario. I would like to thank Dr. George Boer, Chief of the Numerical Modelling Division, for his cheerful hospitality, for numerous stimulating discussions, and, in particular, for his persuasive arguments to shelve the three-dimensional model in favour of this simpler approach.

REFERENCES

Adem, J., 1975: Numerical-thermodynamical prediction of mean monthly ocean temperatures. Tellus, 27, 541-551.

Bathen, K.H., 1971: Heat storage and advection in the North Pacific Ocean. J. Geophys. Res., 76, 676-687.

Bauer, R.W. and M.A. Robinson, 1977: Numerical atlas of oceanographic data, revision 7. Compass Systems Inc., San Diego, California.

Bryan, K. and M.D. Cox, 1972: An approximate equation of state for numerical models of ocean circulation. J. Phys. Ocean., 2, 510-514.

Bryan, K. and E. Schroeder, 1960: Seasonal heat storage in the North Atlantic Ocean. J. Meteor., 17, 670-674.

Bryan, K., S. Manabe and R.C. Pacanowski, 1975: A global ocean-atmosphere climate model. Part II. The oceanic circulation. J. Phys. Ocean., 5, 30-46.

Bunker, A.F., 1976: Computations of surface energy flux and annual air-sea interaction cycles of the North Atlantic Ocean. Mon. Wea. Rev., 1-4, 1122-1140.

Bunker, A.F. and R.A. Goldsmith, 1979: Archived time series of Atlantic Ocean meteorological variables and surface fluxes. Woods Hole Oceanogr. Inst., Tech. Rept., WHOI-79-3, 28 pp.

Bunker, A.F. and L.V. Worthington, 1976: Energy exchange charts of the North Atlantic Ocean., Bull. Amer. Meteor. Soc., 57, 670-678.

Canada Centre for Inland Waters, 1979: Assessment of water quality simulation capability for Lake Ontario. CCIW, Burlington, Ont., Scientific Series No. 111, 220 pp.

Ekman, V.W., 1905: On the influence of the earth's rotation on ocean currents. Ark. Mat. Astr. Fys., 2 (11), 52 pp.

Fissel, D., S. Pond and M. Miyaki, 1977: Computation of surface fluxes from climatological and synoptic data. Mon. Wea. Rev., 105, 26-36.

Fofonoff, N.P., 1962: Machine computations of mass transport in the North Pacific Ocean. J. Fish. Res. Bd. Can., 19, 1121-1141.

Fofonoff, N.P. and S. Tabata, 1966: Variability of oceanographic conditions between ocean station P and Swiftshore Bank off the Pacific Coast of Canada. J. Fish. Res. Bd. Can., 23, 825-868.

Friedrich, H. and S. Levitus, 1972: An approximation to the equation of state for sea water, suitable for numerical ocean models. J. Phys. Ocean., 2, 514-517.

Garwood, R.W., 1977: An oceanic mixed layer model capable of simulating cyclic states. J. Phys. Ocean., 7, 455-468.

Gill, A.E. and P.P. Niiler, 1973: The theory of the seasonal variability in the ocean. Deep-Sea Res.. 20, 141-177.

Gill, A.E. and J.S. Turner, 1976: A comparison of seasonal thermocline models with observation. Deep-Sea Res., 23, 391-401.

Haney, R.L., 1980: A numerical case study of the development of large-scale thermal anomalies in the central North Pacific Ocean. J. Phys. Ocean., 10, 541-556.

Haney, R.L. and R.W. Davies, 1976: The role of surface mixing in the seasonal variation of the ocean thermal structure. J. Phys. Ocean., 6, 504-510.

Hellerman, S., 1967: An updated estimate of the wind stress on the world ocean. Mon. Wea. Rev., 95, 607-626; Correction, Mon. Wea. Rev., 96, 63-74.

Jacob, W.J., 1967: Numerical semiprediction of monthly mean sea surface temperature. J. Geophys. Res., 72, 1681-1689.

Karelse, M., C.B. Vreugdenhil and G.A.L. Delvigne, 1974: Momentum and mass transfer in stratified flows. Delft Hydraul. Lab., Delft, The Netherlands, Rept. R880, 143 pp.

Kim, J.W., 1976: A generalized bulk model of the oceanic mixed layer. J. Phys. Ocean., 6, 686-695.

Kim, J.W. and W.L. Gates, 1979: The annual variability of sea surface temperatures: observation and simulation. WHO, Geneva, GARP Publ. Ser. No. 22, 688-714.

Kraus, E.B. and J.S. Turner, 1967: A one-dimensional model of the seasonal thermocline: II. The general theory and its consequences. Tellus, 19, 98-105.

Kundu, P.K., 1980. A numerical investigation of mixed layer dynamics. J. Phys. Ocean., 10, 220-236.

Leetmaa, A. and A.F. Bunker, 1978: Updated charts of the mean annual wind stress, convergences in the Ekman layers, and Sverdrup transports in the North Atlantic. J. Mar. Res., 36, 311-322.

Mellor, G.L. and P.A. Durbin, 1975: The structure and dynamics of the ocean surface mixed layer. J. Phys. Ocean., 5, 718-728.

Mellor, G.L. and T. Yamada, 1974: A hierarchy of turbulent closure models for planetary boundary layers. J. Atmos. Sci., 31, 1781-1806.

Meyers, G., 1975: Seasonal variation in the transport of the Pacific North Equatorial Current relative to the wind field. J. Phys. Ocean., 5, 442-449.

Munk, W.H. and E.R. Anderson, 1948: Notes on a theory of the thermocline. J. Mar. Res., 7, 276-295.

Namias, J., 1965: Macroscopic association between mean monthly sea-surface temperature and overlying winds. J. Geophys. Res., 70, 2307-2318.

Namias, J., 1972: Experiments in objectively predicting some atmospheric and oceanic variables for the winter of 1971-72. J. Appl. Meteor., 11, 1164-1174.

Niiler, P.P. and E.B. Kraus, 1977: One-dimensional models of the upper ocean. Modelling and Prediction of the Upper Layers of the Ocean (E.B. Kraus, Ed.), Pergamon Press, 143-172.

Oort, A.H. and T.H. Vonder Haar, 1976: On the observed annual cycle in the ocean-atmosphere heat balance over the northern hemisphere. J. Phys. Ocean., 6, 781-800.

Schopf, P.S., 1980: The role of Ekman flow and planetary waves in the oceanic cross-equatorial heat transport. J. Phys. Ocean., 10, 330-341.

Schutz, C. and W.L. Gates, 1971: Global climatic data for surface, 800 mb, 400 mb for January. Rand Corp., Santa Monica, Cal., Tech. Rept. R-915-ARPA, 173 pp.

Schutz, C. and W.L. Gates, 1972: Global climatic data for surface, 800 mb, 400 mb for July. Rand Corp., Santa Monica, Cal., Tech. Rept. R-1029-ARPA, 180 pp.

Schutz, C. and W.L. Gates, 1973: Global climatic data for surface, 800 mb, 400 mb for April. Rand Corp., Santa Monica, Cal., Tech. Rept. R-1317-ARPA, 192 pp.

Schutz, C. and W.L. Gates, 1974: Global climatic data for surface, 800 mb, 400 mb for October. Rand Corp., Santa Monica, Cal., Tech. Rept. R-1425-ARPA, 192 pp.

Simons, T.J., 1980: Verification of seasonal stratification models. Univ. of Utrecht, Netherlands, Inst. Meteorol. Oceanogr., 15 pp.

Sundaram, T.R. and R.G. Rehm, 1973: The seasonal thermal structure of deep temperate lakes. Tellus, 25, 157-167.

Thompson, R.O.R.Y., 1976: Climatological numerical models of the surface mixed layer of the ocean. J. Phys. Ocean., 6, 496-503; 7, 470-471.

Veronis, G. and H. Stommel, 1956: The action of variable wind stresses on a stratified ocean. J. Mar. Res., 15, 43-75.

Walters, R.A., G.F. Carey and D.R. Winter, 1978: Temperature computations for temperate lakes. App. Math. Modelling, 2, 41-47.

Wells, N.C., 1979: A coupled ocean-atmosphere experiment. The ocean response. Q.J. Royal Meteor. Soc., 105, 335-370.

Wetherald, R.T. and S. Manabe, 1972: Response of the joint ocean-atmosphere model to the seasonal variation of the solar radiation. Mon. Wea. Rev., 100, 42-57.

White, W.B., 1977: Annual forcing of baroclinic long waves in the tropical North Pacific Ocean. J. Phys. Ocean., 7, 50-61.

White, W.B., 1978: A wind-driven model experiment of the seasonal cycle of the main thermocline in the interior midlatitude North Pacific. J. Phys. Ocean., 18, 818-824.

White, W.B., R.L. Bernstein, G. McNally and S. Pazan, 1980: The thermocline response to transient atmospheric forcing in the interior midlatitude North Pacific. J. Phys. Ocean., 10, 372-384.

FIGURE LEGENDS

Fig. 1a. Rate of heat storage in upper ocean for January from Bauer-Robinson (1977) and total downward heat flux at the ocean surface from Schutz and Gates (1971).

Fig. 1b. Rate of heat storage in upper ocean for July from Bauer-Robinson (1977) and total downward heat flux at the ocean surface from Schutz and Gates (1971).

Fig. 2 Top: Rate of heat storage according to Bauer-Robinson (1977), shown by solid lines, compared with values of Oort and Vonder Haar (1975) shown by dashed lines.

Bottom: Downward heat flux at ocean surface from Schutz and Gates (1971-1974), shown by solid lines, compared with values from Oort and Vonder Haar (1975) shown by dashed lines. Points indicate values averaged over ocean areas of 10° latitude belts.

Fig. 3a Annual mean convergence of total heat transport obtained from the surface heat balance (top) and heat convergence in upper ocean due to horizontal plus vertical Ekman transports (bottom).

Fig. 3b. Annual mean convergence of total heat transport minus Ekman transport (top) and heat advection by Bathen's (1971) North Pacific stream function (bottom).

Fig. 4. Left: Annual mean downward heat flux at ocean surface zonally averaged over all oceans and over Atlantic and Pacific separately.

Right: Annual means of convergence of heat transport by Ekman currents (solid lines) and heat advection by Bathen's (1971) North Pacific stream function (dashed line).

Fig. 5a. Seasonal deviation from annual mean convergence of heat transport for January obtained from the rate of heat storage and the surface heat flux (top) and corresponding heat convergence by horizontal plus vertical Ekman advection (bottom).

Fig. 5b. Seasonal deviation from annual mean convergence of heat transport for July obtained from the rate of heat storage and the surface heat flux (top) and corresponding heat convergence by horizontal plus vertical Ekman advection (bottom).

Fig. 6a. Left: January deviations from annual means of downward surface heat flux (solid lines) and rate of heat storage (dashed) zonally averaged over all oceans and over Atlantic and Pacific separately.
Right: Corresponding values of convergence of total heat transport (dashed) and convergence of Ekman heat transports (solid lines).

Fig. 6b. Left: July deviations from annual means of downward surface heat flux (solid lines) and rate of heat storage (dashed) zonally averaged over all oceans and over Atlantic and Pacific separately.
Right: Corresponding values of convergence of total heat transport (dashed) and convergence of Ekman heat transports (solid lines).

Fig. 7. Components of seasonal deviations of horizontal (dashed) and vertical (solid) advection of heat by Ekman current for January (left) and July (right).

Top: Seasonally varying part of product of current and temperature.
Middle: Contribution from seasonal current and annual temperature.
Bottom: Effect of annual current and seasonal temperature.

Fig. 8. Response of stratified surface layer to sudden wind stress as computed by equations (16), (17), (31) and (32).

Left: Results for $\tau=2$ dynes/cm^2 and $\sigma=4$ at various times measured by inertial period $P=2\pi/f$.
Middle: Corresponding values of eddy diffusivity (solid lines) and its neutral value (dashes).
Right: Results after 10 inertial periods for different τ and σ.

Fig. 9. Observed temperatures in Lake Ontario (solid lines) and results obtained from present model with prescribed surface heat flux and wind stress (dashes).

Fig. 10. Latitudinal variations of seasonal wind stress for the North Atlantic near 40°W (above) and for the North Pacific near 170°W (below). Solid curves: monthly means of stress magnitude; dashes: magnitude of vector-averaged stress from Hellerman (1967); long dashes: magnitude of vector-averaged stress from revised U.S. Navy Marine Climatic Atlas (1974-77).

Fig. 11. Seasonal variations of components of upper ocean heat budget as given by equation (11a) and observed upper ocean temperatures for 10 degree squares in the North Atlantic, 30 to 40°W.

Fig. 12. Seasonal variations of components of upper ocean heat budget as given by equation (11a) and observed upper ocean temperatures for 10 degree squares in the North Pacific, 170 to 180°W.

Fig. 13. Sea surface temperatures computed by stratification model for the North Atlantic locations of Fig. 11.

Left Panel: Solid curves show results from basic experiment with stability parameter σ=1, variable Coriolis parameter and excluding annual mean components of surface heat flux Q, Ekman heat advection E, and residual term in heat budget R (see equations 14a-b); dashed curves present results for constant Coriolis parameter; long dashes for stability parameter σ=2.

Middle Panel: Solid curves obtained without Ekman effect (E'=0); dashes without residual term (R'=0); long dashes with residual term R' included in surface heat flux Q'.

Right Panel: Solid curves show results without Ekman effect (E'=0) but including annual mean components of surface heat flux Q and residual term R; dashed curves same as solid ones but including seasonal and annual mean Ekman effects (E+E'); long dashes: same as basic experiment but constant diffusion coefficient of 1.5 cm^2/s for stable conditions.

Fig. 14. Sea surface temperatures computed by stratification model for the North Pacific locations of Fig. 12.

Left Panel: Solid curves show results from basic experiment with stability parameter σ=1, variable Coriolis parameter and excluding annual mean components of surface heat flux Q, Ekman heat advection E, and residual term in heat budget R (see equations 14a-b); dashed curves present results for constant Coriolis parameter; long dashes for stability parameter σ=2.

Middle Panel: Solid curves obtained without Ekman effect (E'=0); dashes without residual term (R'=0); long dashes with residual term R' included in surface heat flux Q'.

Right Panel: Solid curves show results without Ekman effect (E'=0) but including annual mean components of surface heat flux Q and residual term R; dashed curves same as solid ones but including seasonal and annual mean Ekman effects (E+E'); long dashes: same as basic experiment but constant diffusion coefficient of 1.5 cm^2/s for stable conditions.

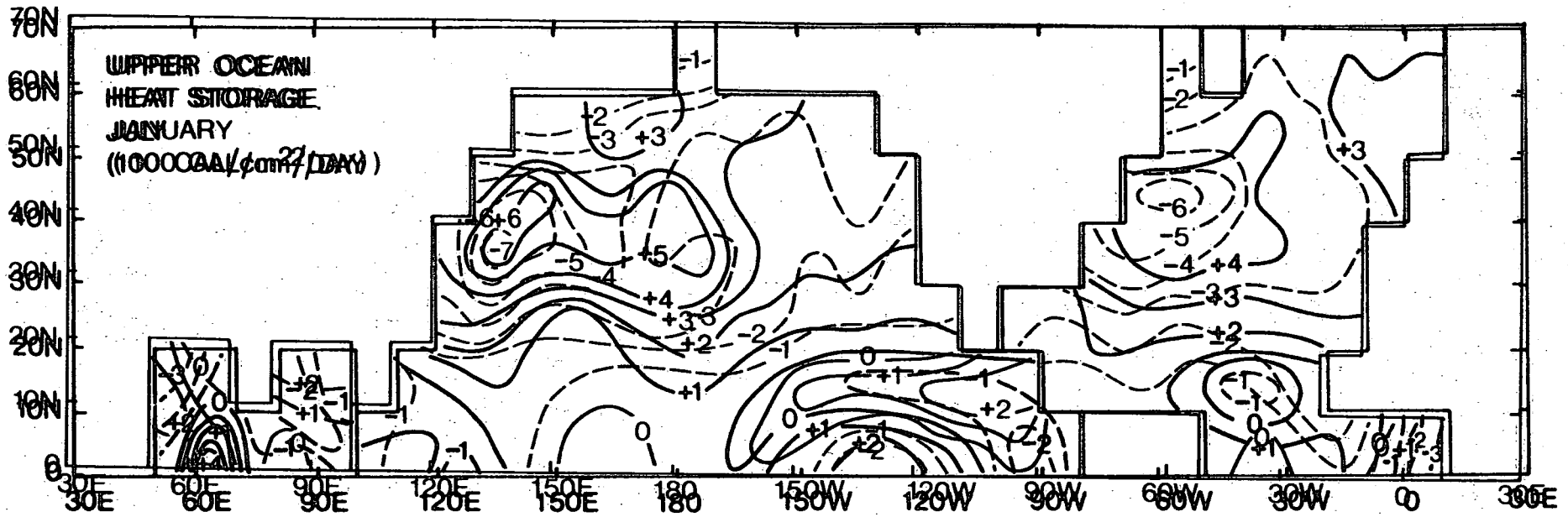
UPPER OCEAN
HEAT STORAGE
JANUARY
(100 CAL/cm²/DAY)
70N
60N
50N
40N
30N
20N
10N
0
30E
60E
90E
120E
150E
180
150W
120W
90W
60W
30W
0
30E

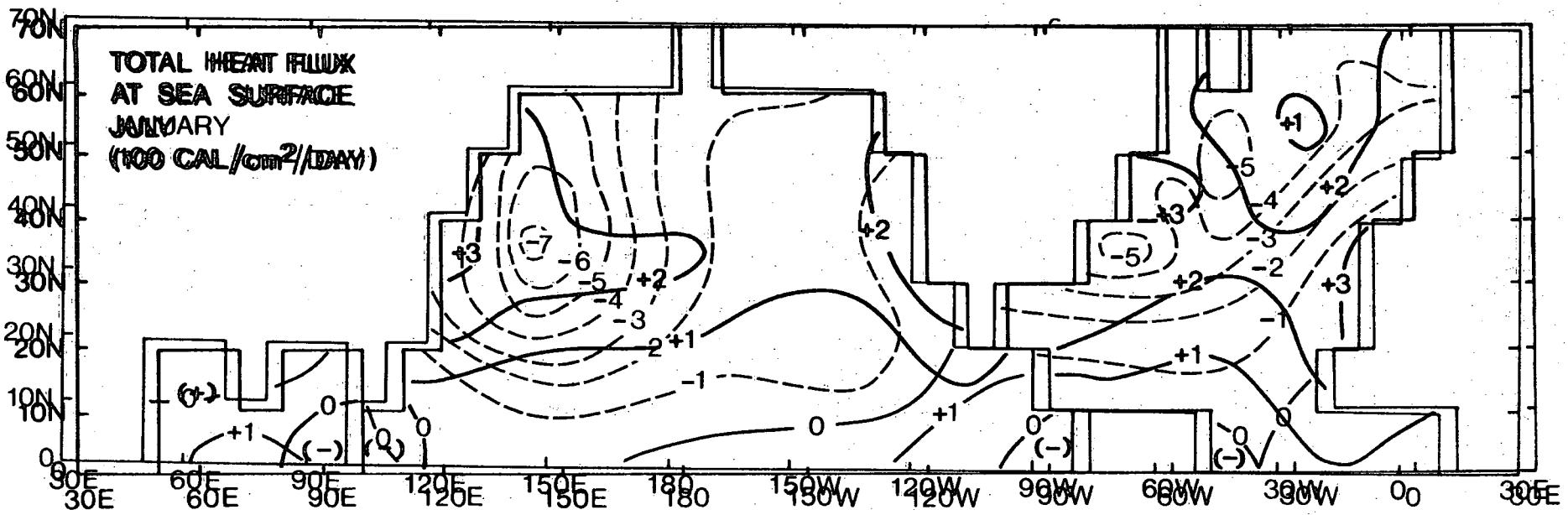
TOTAL HEAT FLUX
AT SEA SURFACE
JANUARY
(100 CAL/cm²/DAY)
70N
60N
50N
40N
30N
20N
10N
0
30E
60E
90E
120E
150E
180
150W
120W
90W
60W
30W
0
30E

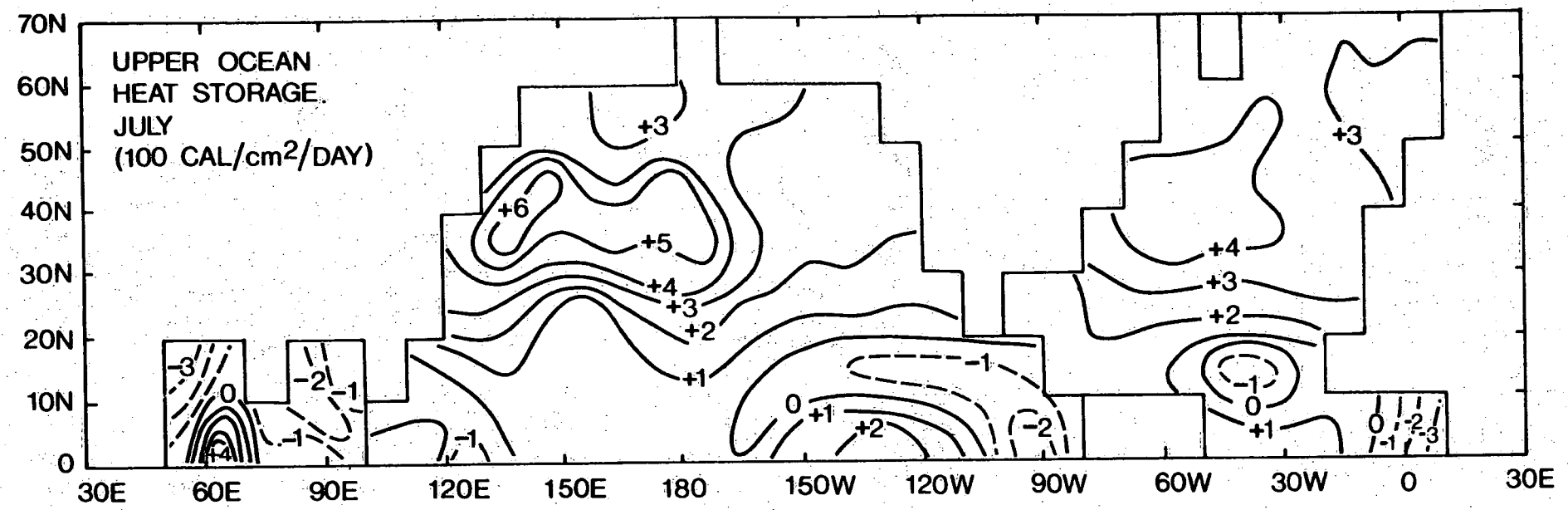
UPPER OCEAN
HEAT STORAGE.
JULY
(100 CAL/cm2/DAY)
70N
60N
50N
40N
30N
20N
10N
0
30E
60E
90E
120E
150E
180
150W
120W
90W
60W
30W
0
30E

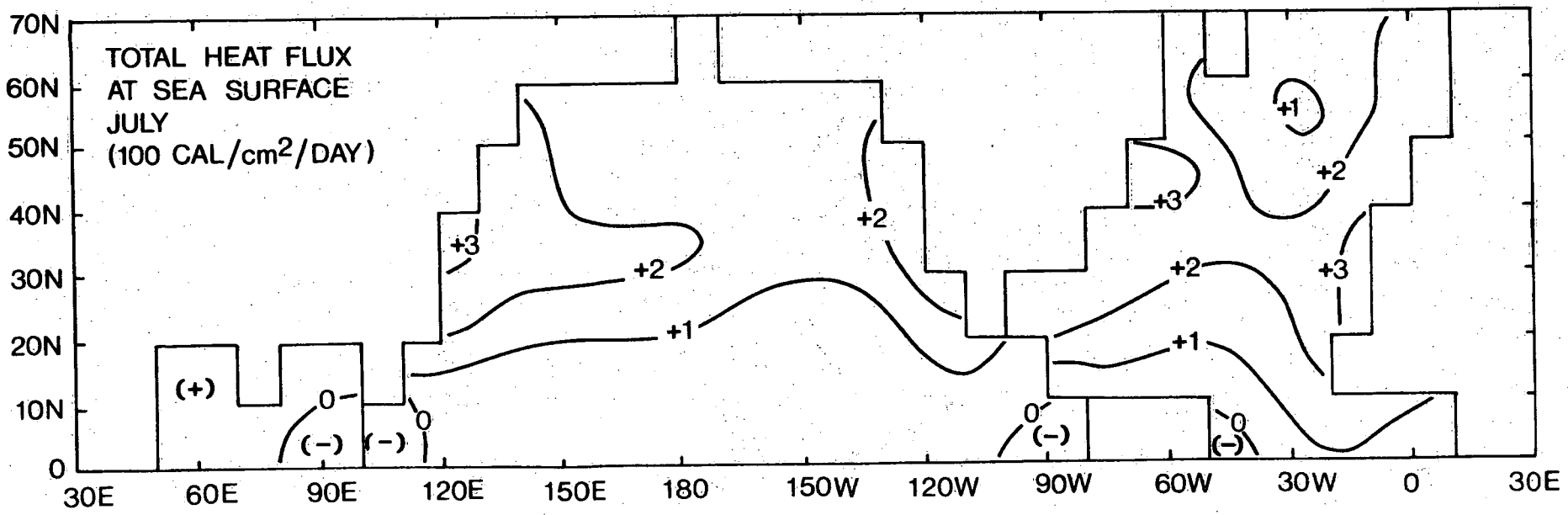
TOTAL HEAT FLUX
AT SEA SURFACE
JULY
(100 CAL/cm2/DAY)
70N
60N
50N
40N
30N
20N
10N
0
30E
60E
90E
120E
150E
180
150W
120W
90W
60W
30W
0
30E

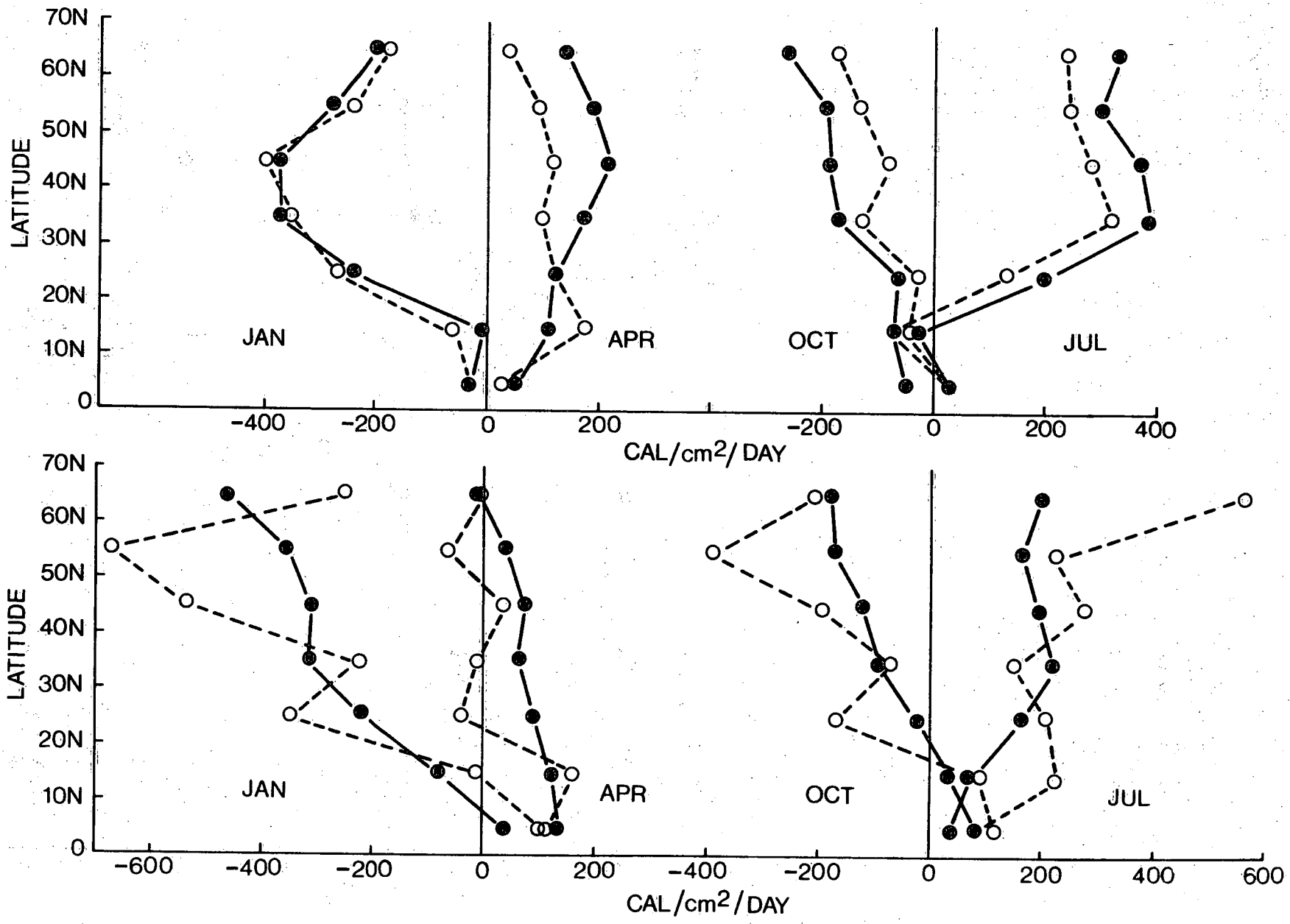
70N
60N
50N
40N
30N
20N
10N
0
LATITUDE
JAN
APR
OCT
JUL
-400
-200
0
200
-200
0
200
400
CAL/cm2/DAY
70N
60N
50N
40N
30N
20N
10N
0
LATITUDE
JAN
APR
OCT
JUL
-600
-400
-200
0
200
-400
-200
0
200
400
600
CAL/cm2/DAY

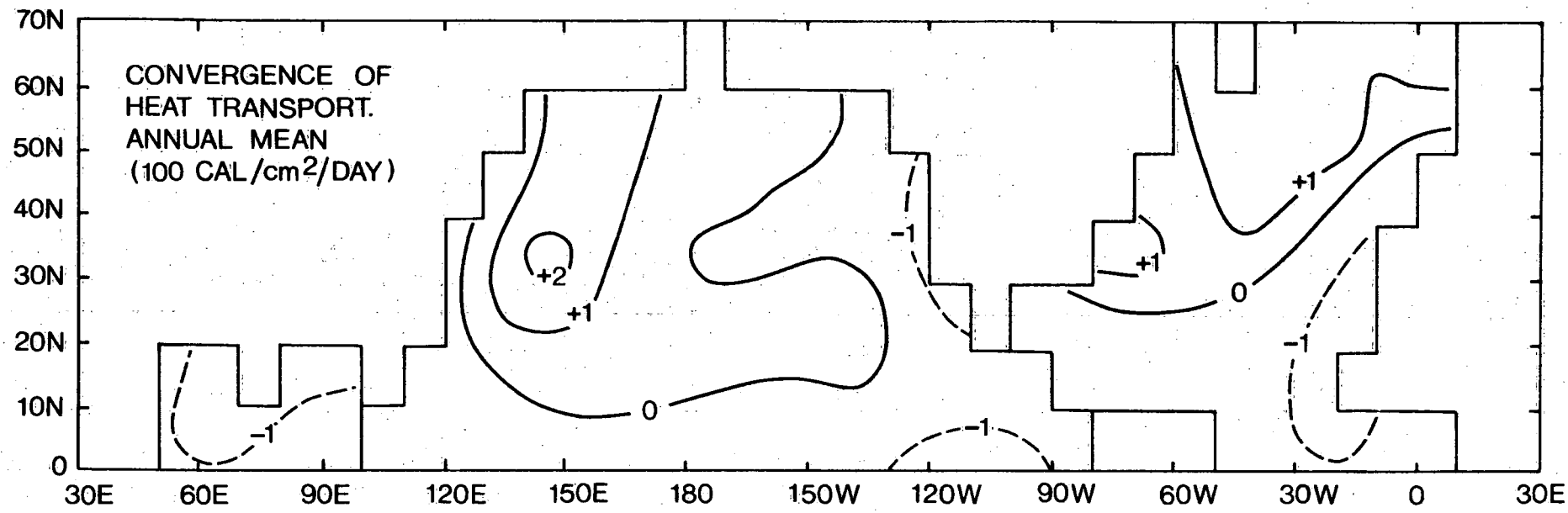
CONVERGENCE OF
HEAT TRANSPORT.
ANNUAL MEAN
(100 CAL/cm2/DAY)
70N
60N
50N
40N
30N
20N
10N
0
30E
60E
90E
120E
150E
180
150W
120W
90W
60W
30W
0
30E
+2
+1
0
-1
-1
-1
+1
+1
0
-1

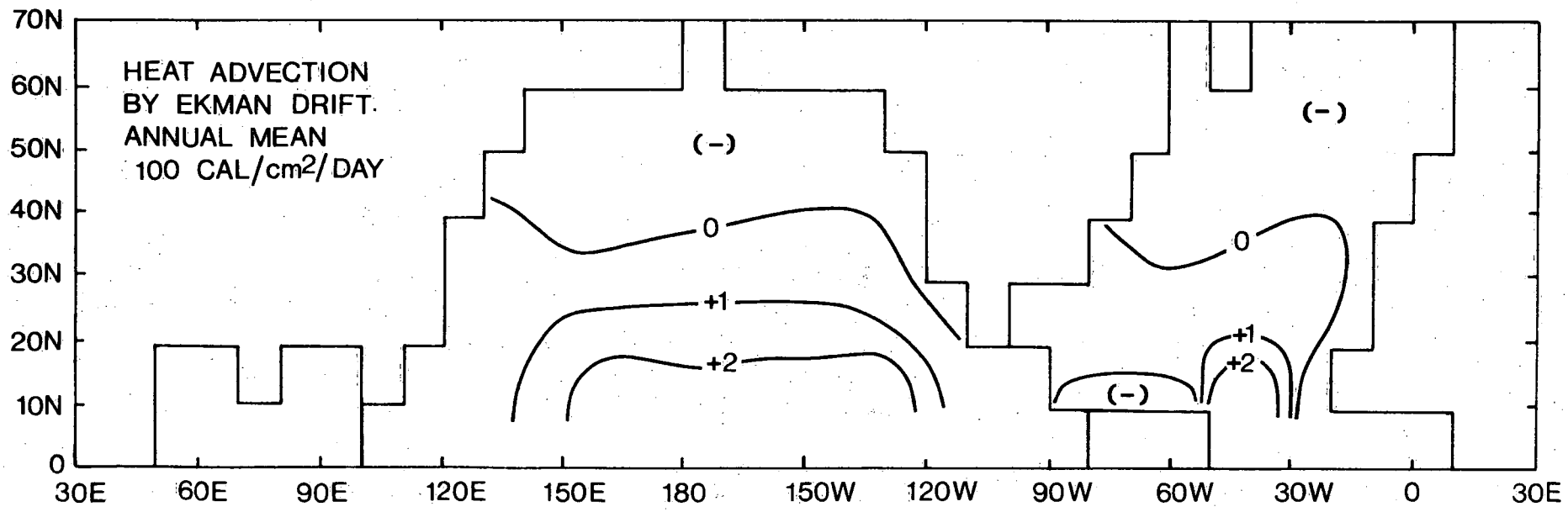
HEAT ADVECTION
BY EKMAN DRIFT.
ANNUAL MEAN
100 CAL/cm2/DAY
70N
60N
50N
40N
30N
20N
10N
0
30E
60E
90E
120E
150E
180
150W
120W
90W
60W
30W
0
30E
(-)
(-)
(-)
0
0
+1
+2
+1
+2

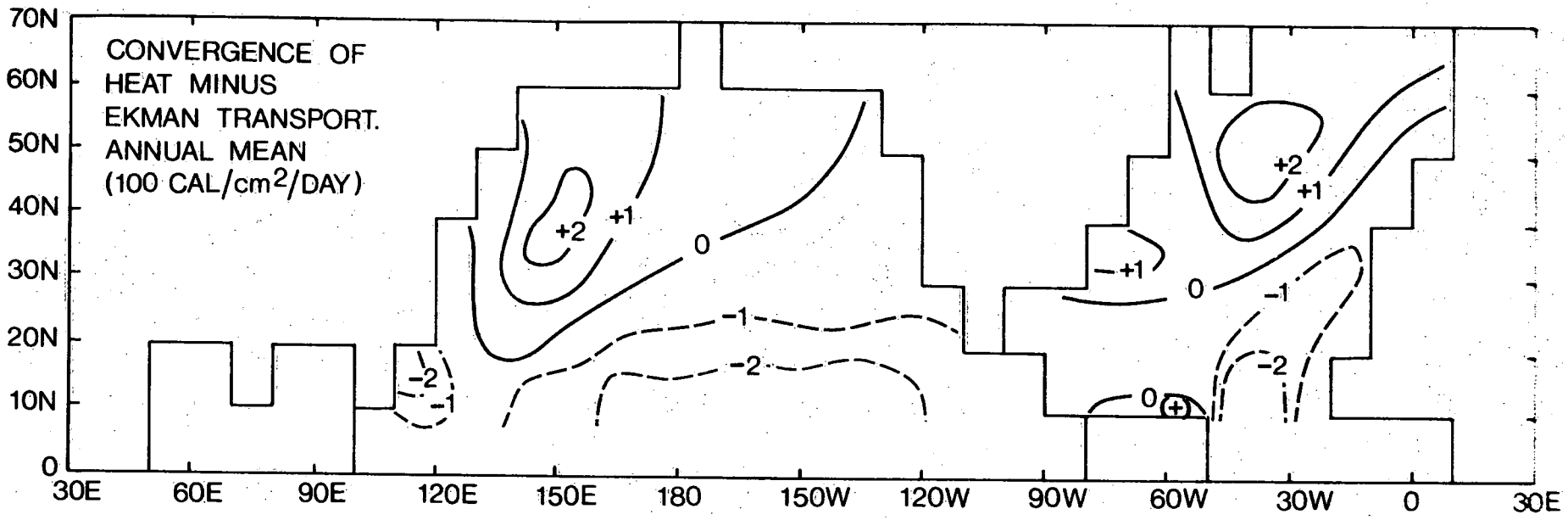
CONVERGENCE OF
HEAT MINUS
EKMAN TRANSPORT.
ANNUAL MEAN
(100 CAL/cm2/DAY)
70N
60N
50N
40N
30N
20N
10N
0
30E
60E
90E
120E
150E
180
150W
120W
90W
60W
30W
0
30E
+2
+1
0
-1
-2
+1
0
-1
-2
+2
+1
0
-2
-1
0
+1

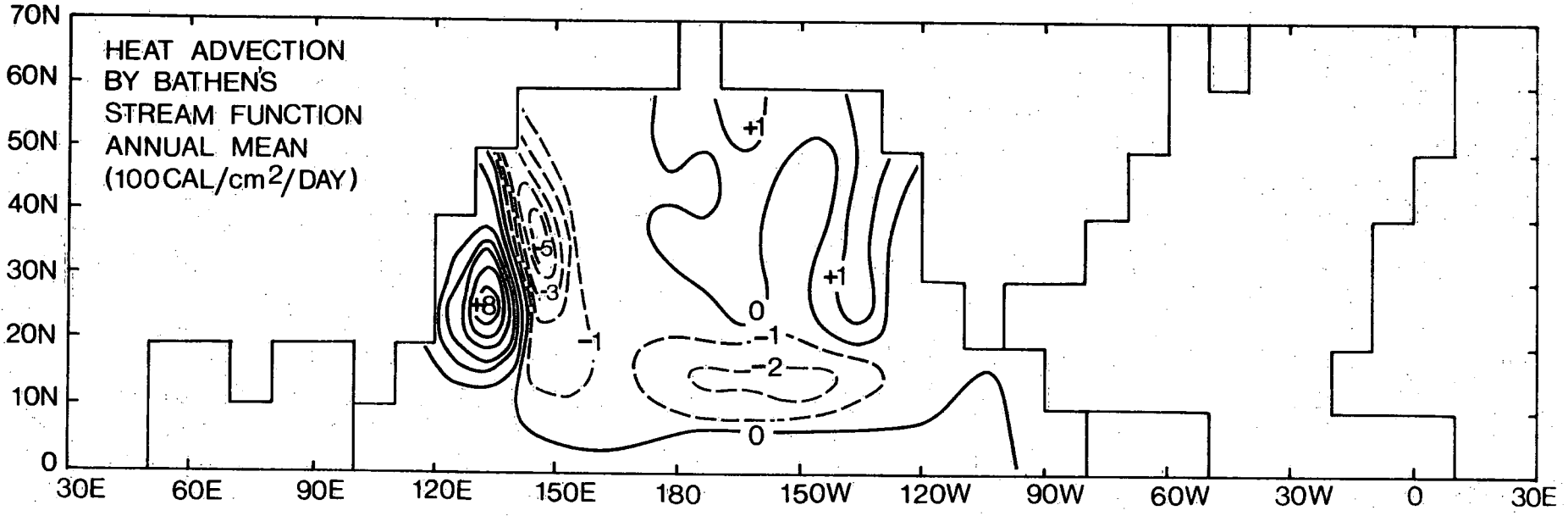
HEAT ADVECTION
BY BATHEN'S
STREAM FUNCTION
ANNUAL MEAN
(100CAL/cm2/DAY)
70N
60N
50N
40N
30N
20N
10N
0
30E
60E
90E
120E
150E
180
150W
120W
90W
60W
30W
0
30E
+1
+1
+5
+3
+8
-1
0
-1
-2
0

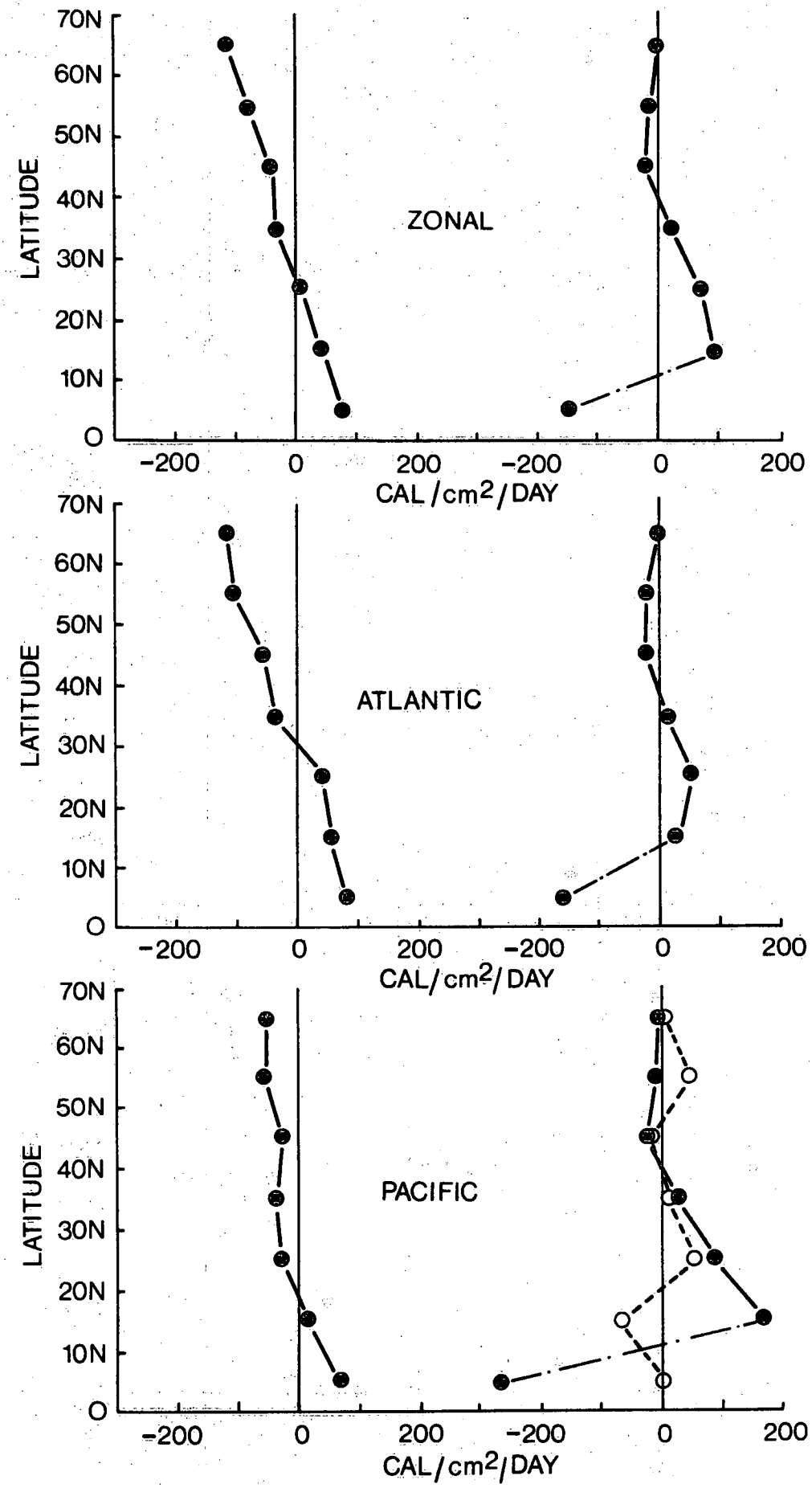
70N
60N
50N
40N
30N
20N
10N
O
LATITUDE
ZONAL
-200
0
200
-200
0
200
CAL/cm2/DAY
ATLANTIC
PACIFIC

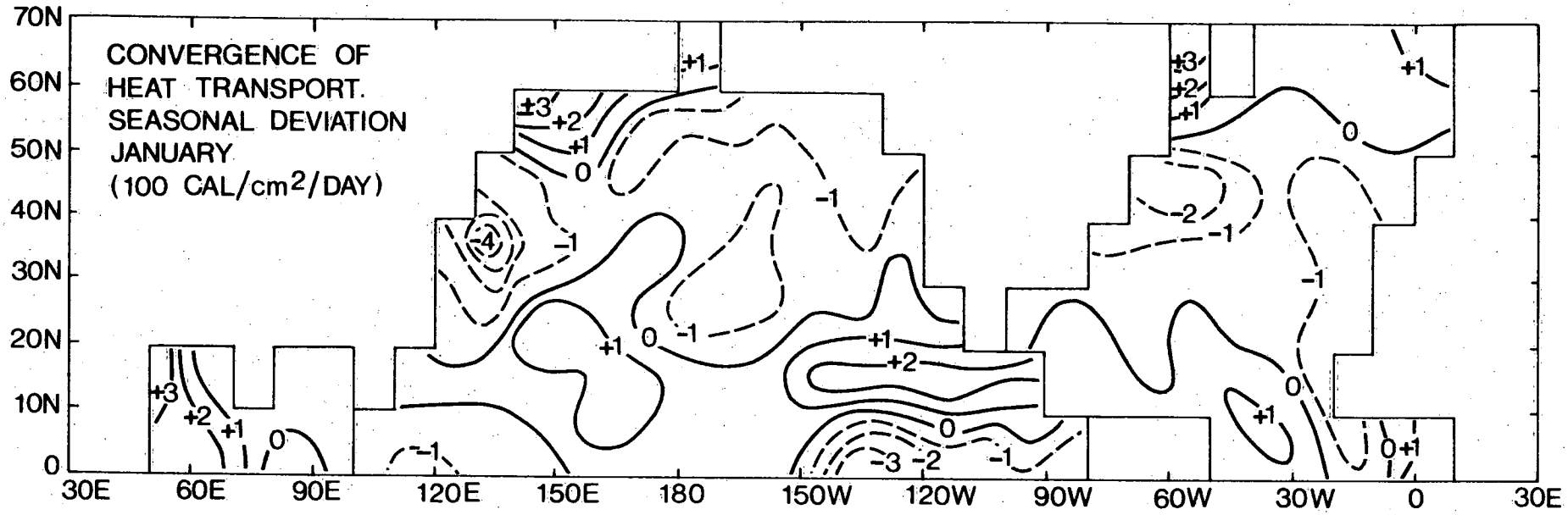
CONVERGENCE OF
HEAT TRANSPORT.
SEASONAL DEVIATION
JANUARY
(100 CAL/cm2/DAY)
70N
60N
50N
40N
30N
20N
10N
0
30E
60E
90E
120E
150E
180
150W
120W
90W
60W
30W
0
30E

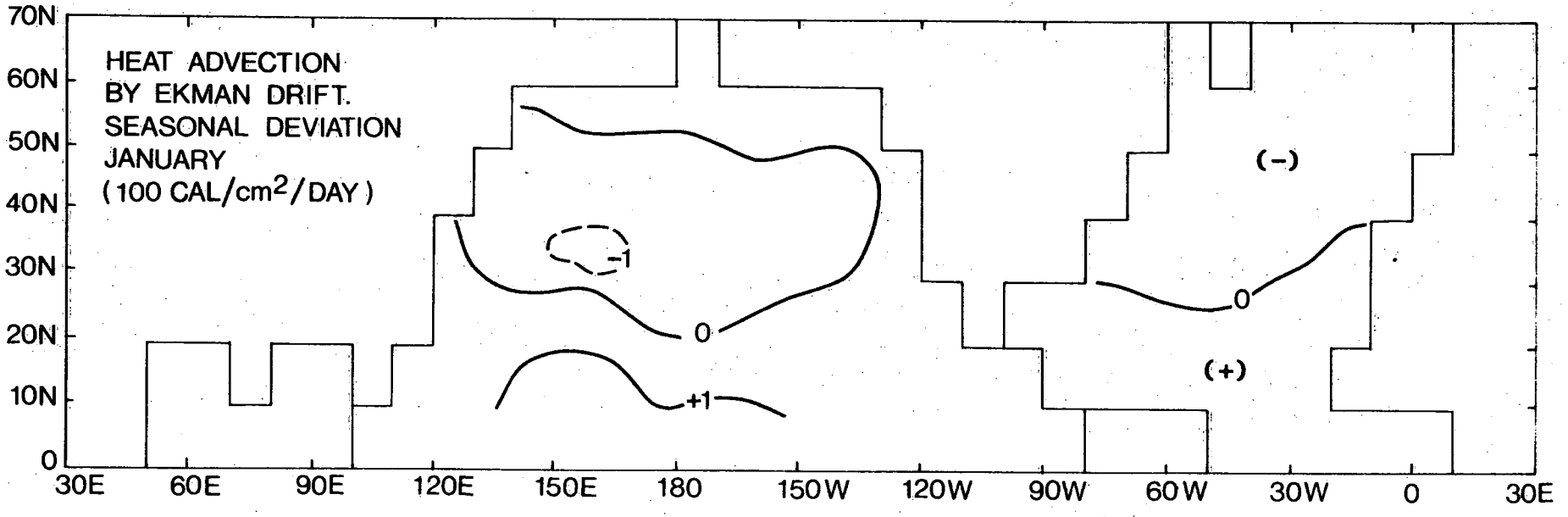
HEAT ADVECTION
BY EKMAN DRIFT.
SEASONAL DEVIATION
JANUARY
(100 CAL/cm2/DAY)
70N
60N
50N
40N
30N
20N
10N
0
(-)
(+)
30E
60E
90E
120E
150E
180
150W
120W
90W
60W
30W
0
30E

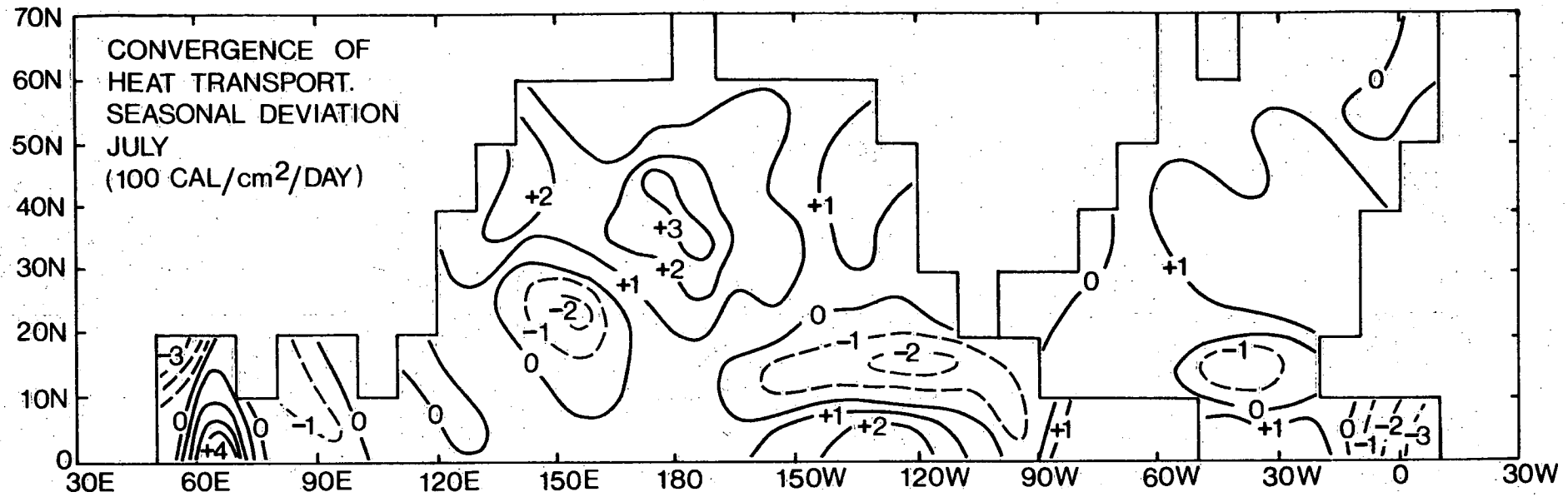
CONVERGENCE OF
HEAT TRANSPORT.
SEASONAL DEVIATION
JULY
(100 CAL/cm2/DAY)
70N
60N
50N
40N
30N
20N
10N
0
30E
60E
90E
120E
150E
180
150W
120W
90W
60W
30W
0
30W

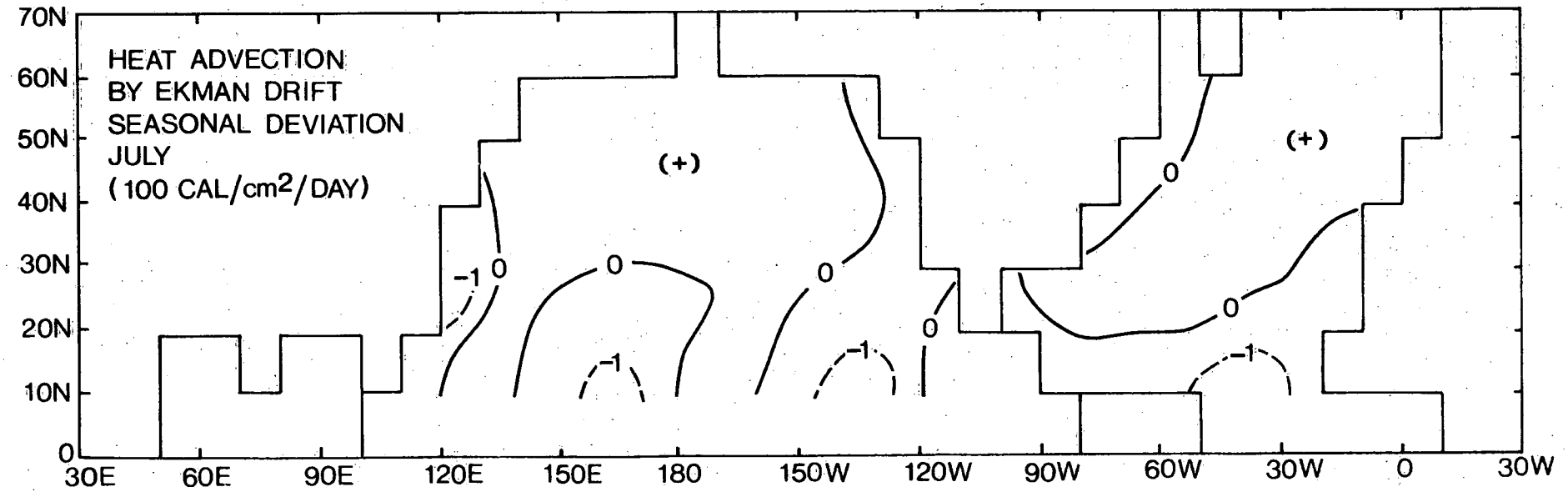
HEAT ADVECTION
BY EKMAN DRIFT
SEASONAL DEVIATION
JULY
(100 CAL/cm2/DAY)
(+)
(+)
70N
60N
50N
40N
30N
20N
10N
0
30E
60E
90E
120E
150E
180
150W
120W
90W
60W
30W
0
30W

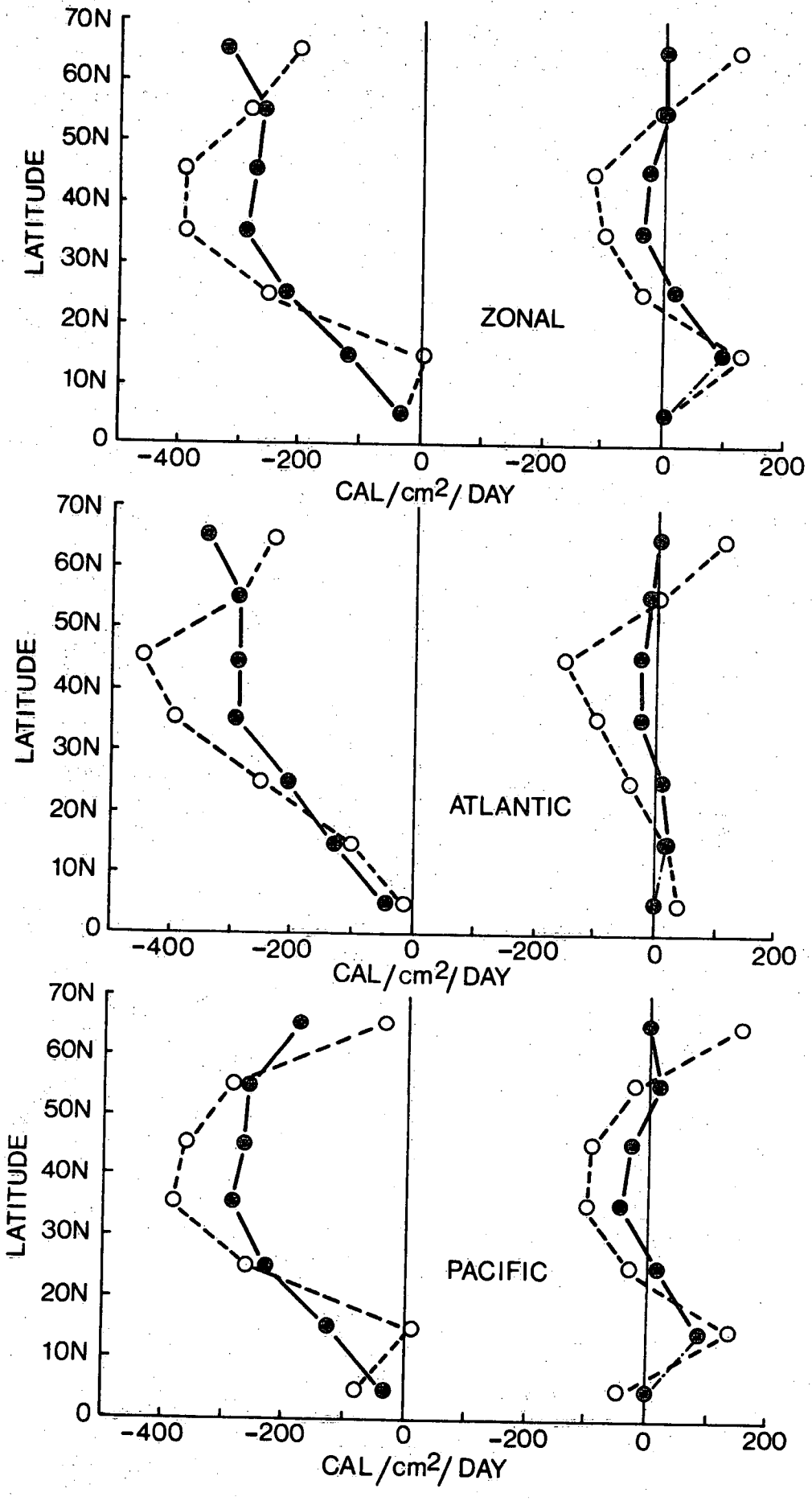
70N
60N
50N
40N
30N
20N
10N
0
LATITUDE
ZONAL
-400
-200
0
-200
0
200
CAL/cm2/DAY
ATLANTIC
PACIFIC

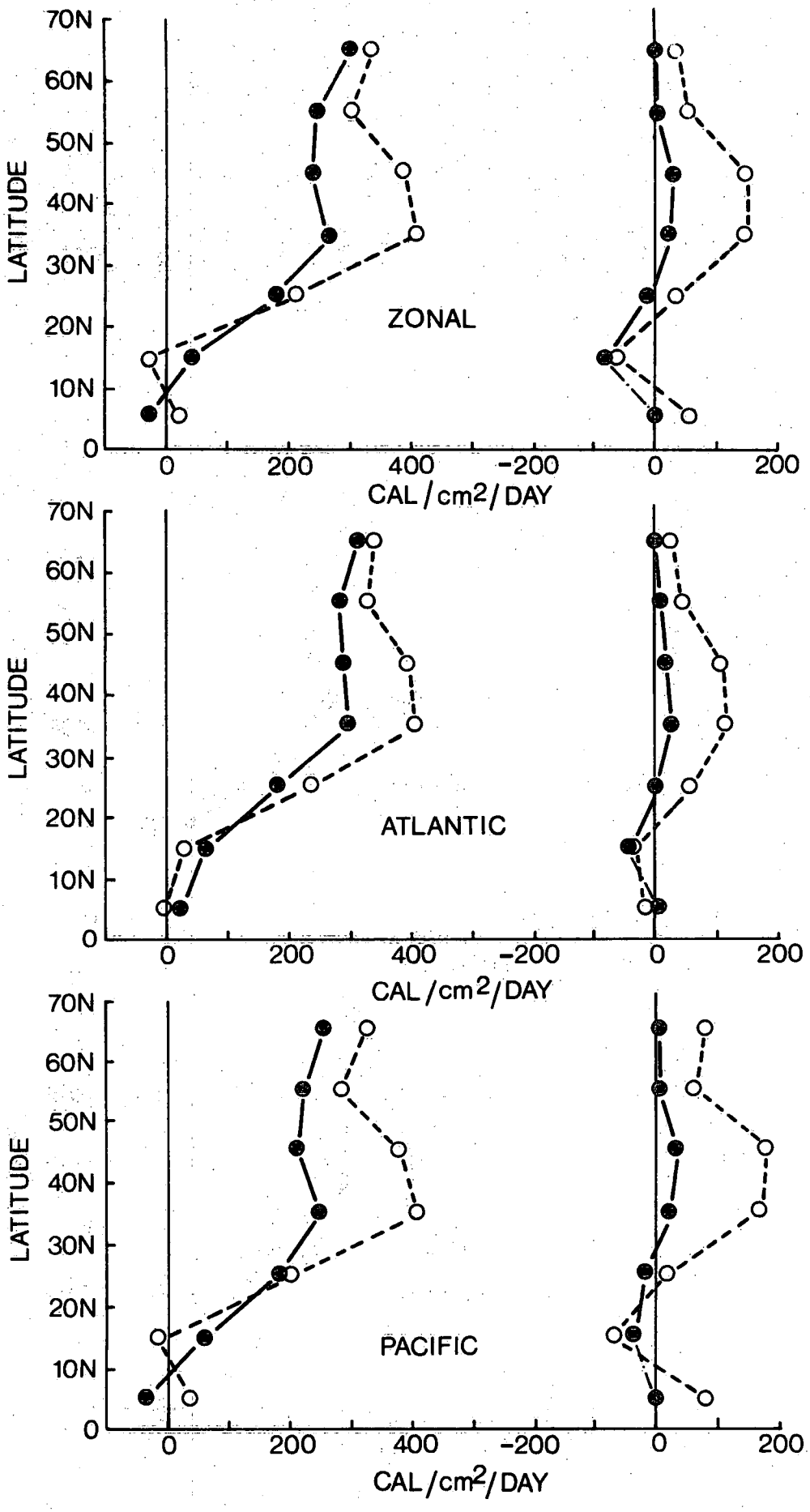
70N
60N
50N
40N
30N
20N
10N
0
LATITUDE
ZONAL
0
200
400
-200
0
200
CAL / cm2 / DAY
ATLANTIC
PACIFIC

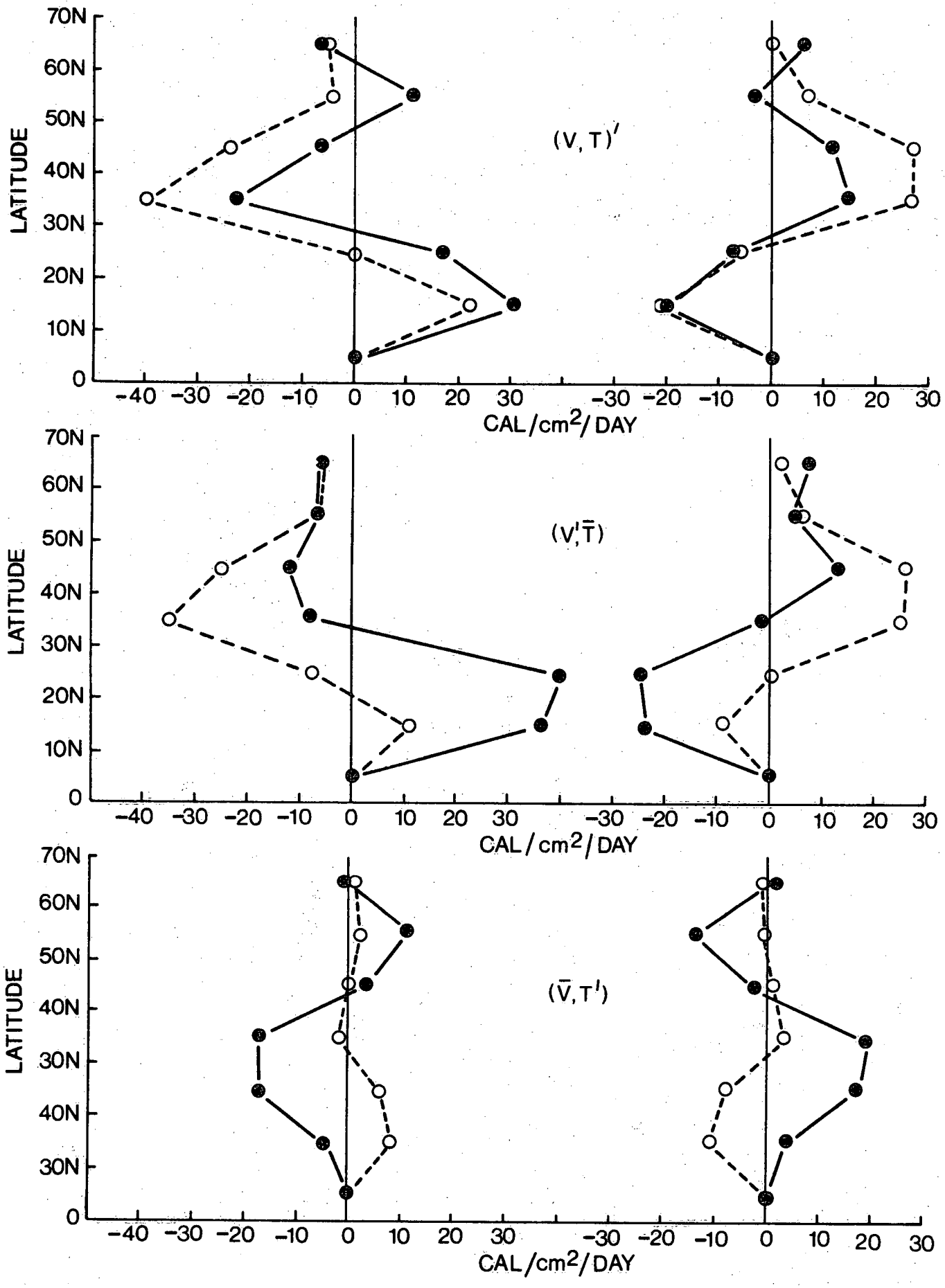
70N
60N
50N
40N
30N
20N
10N
0
LATITUDE
(V, T)′
(V′,T̄)
(V̄,T′)
-40 -30 -20 -10 0 10 20 30
-30 -20 -10 0 10 20 30
CAL/cm²/DAY

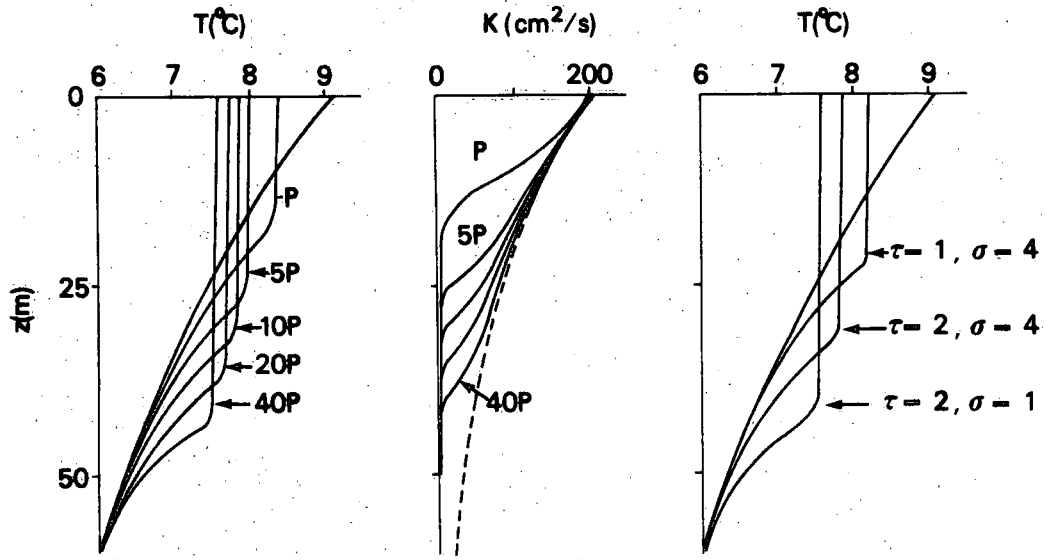
T(°C)
K (cm²/s)
T(°C)
6 7 8 9
0 200
6 7 8 9
0
25
50
z(m)
P
5P
10P
20P
40P
P
5P
40P
τ= 1, σ = 4
τ= 2, σ = 4
τ= 2, σ = 1

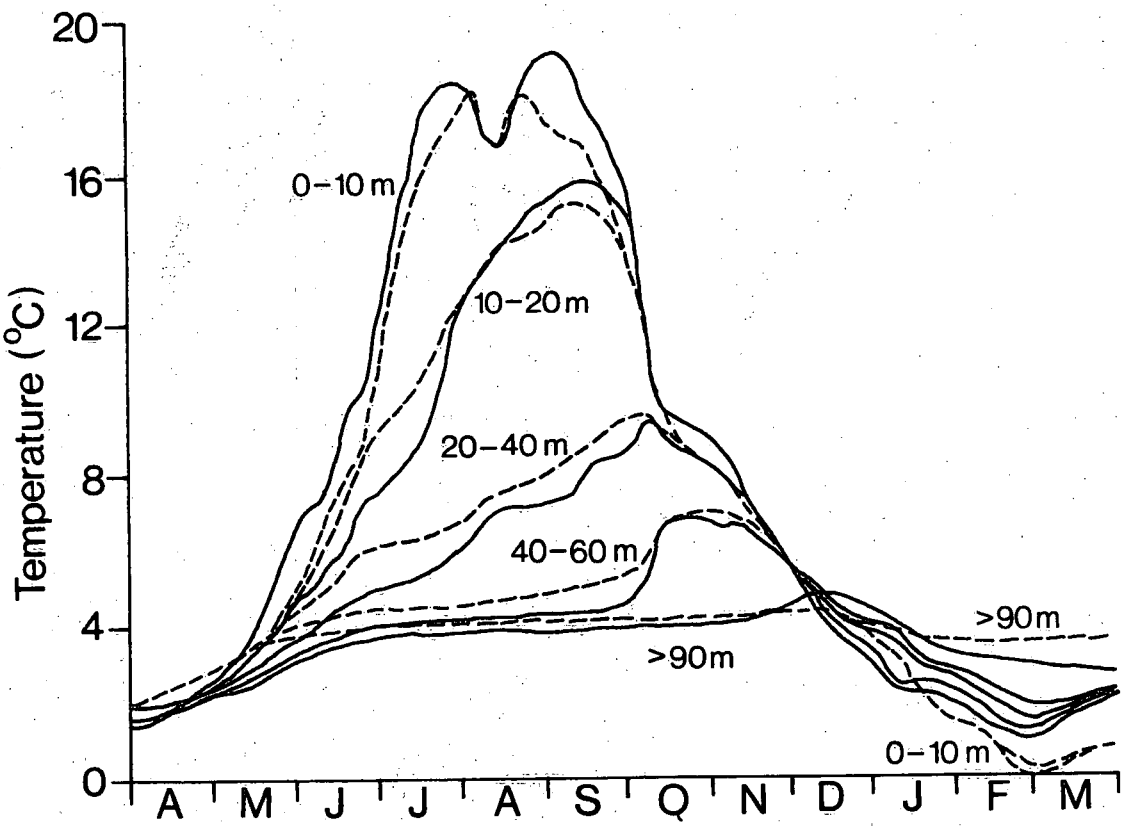
20
16
12
8
4
0
Temperature (°C)
0–10 m
10–20 m
20–40 m
40–60 m
>90m
>90m
0–10 m
A M J J A S Q N D J F M

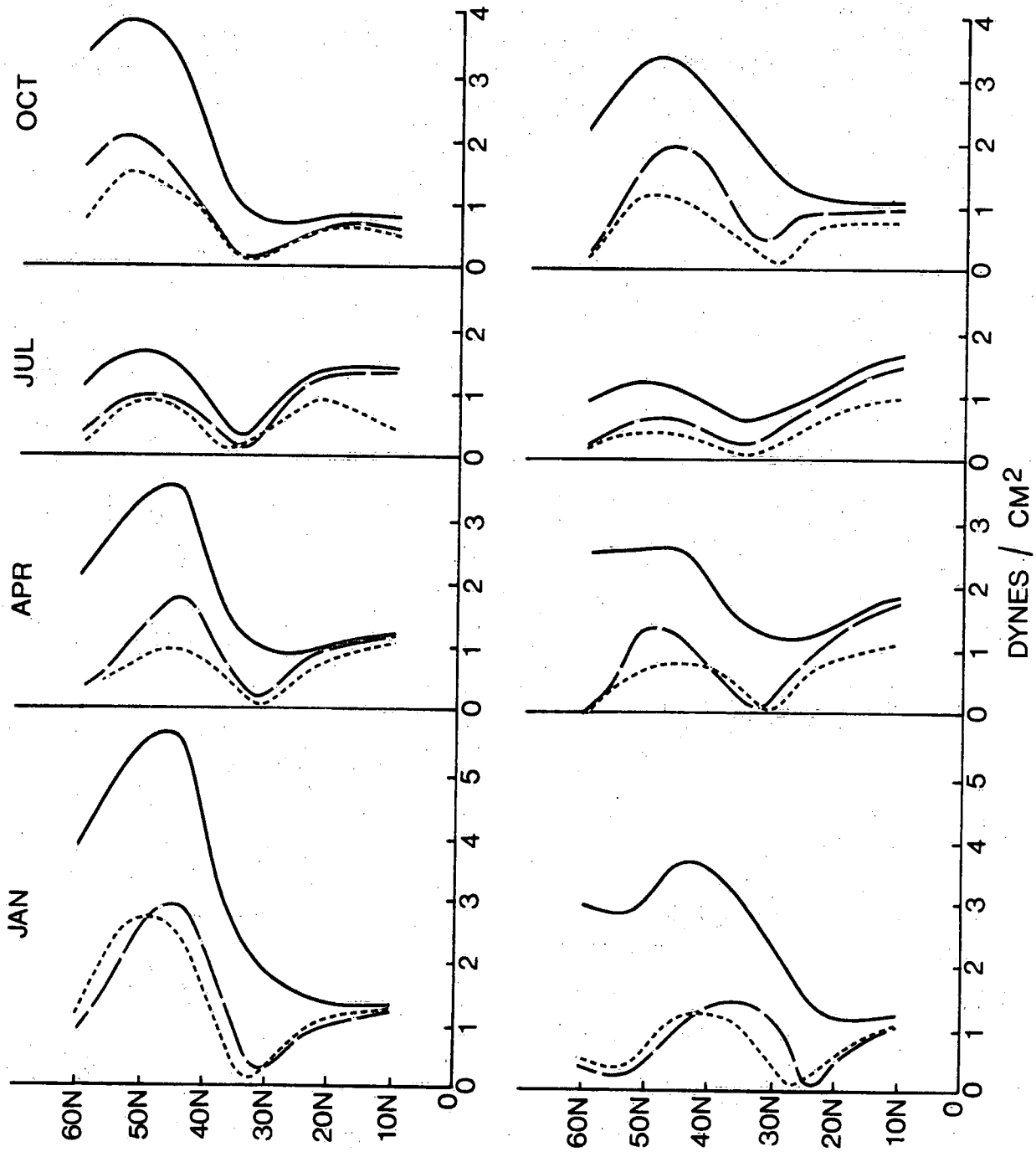
OCT
JUL
APR
JAN
60N
50N
40N
30N
20N
10N
0
1
2
3
4
5
DYNES / CM2

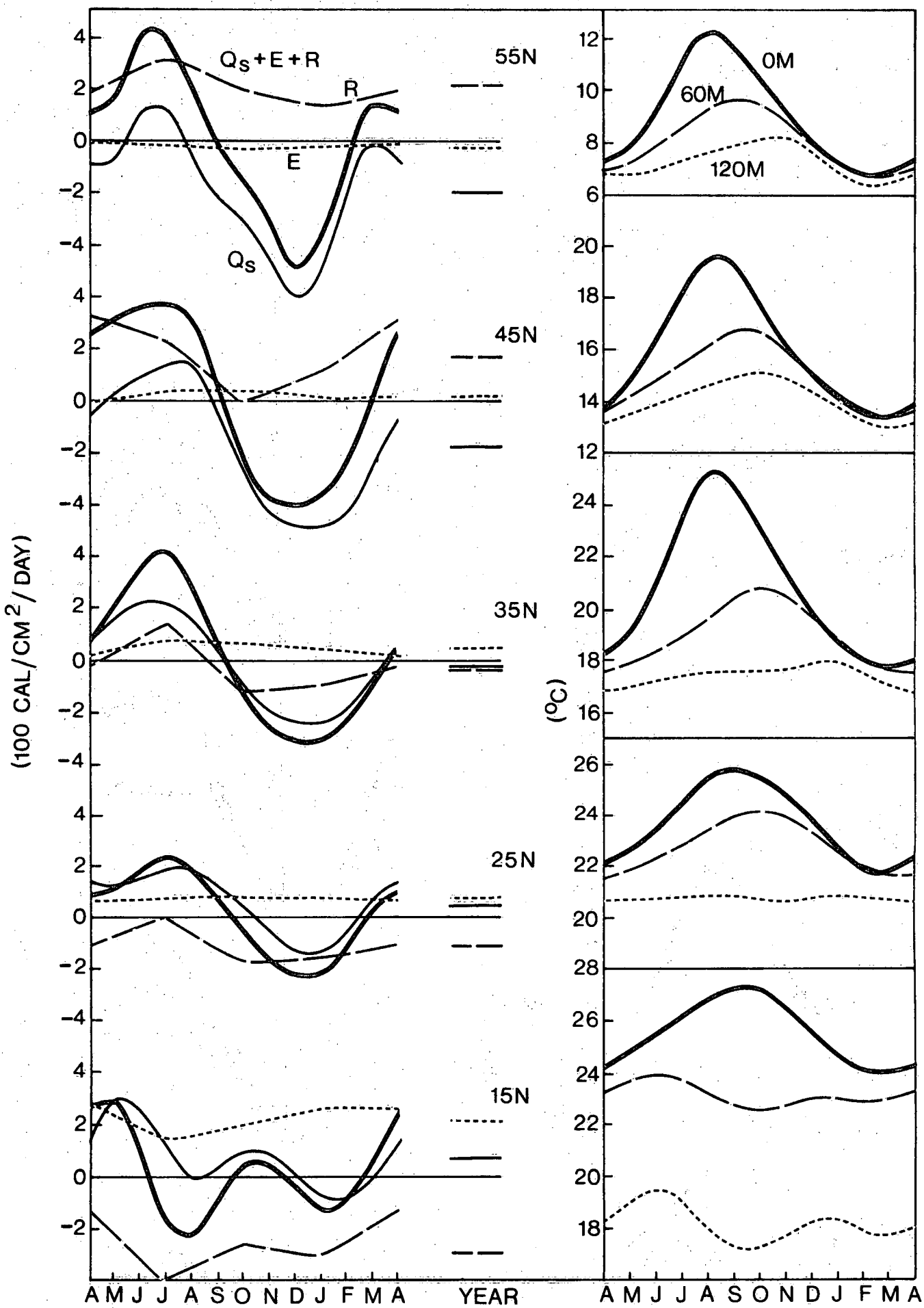
Qs+E+R
R
E
Qs
55N
45N
35N
25N
15N
0M
60M
120M
(100 CAL/CM2/DAY)
(°C)
A M J J A S O N D J F M A
YEAR

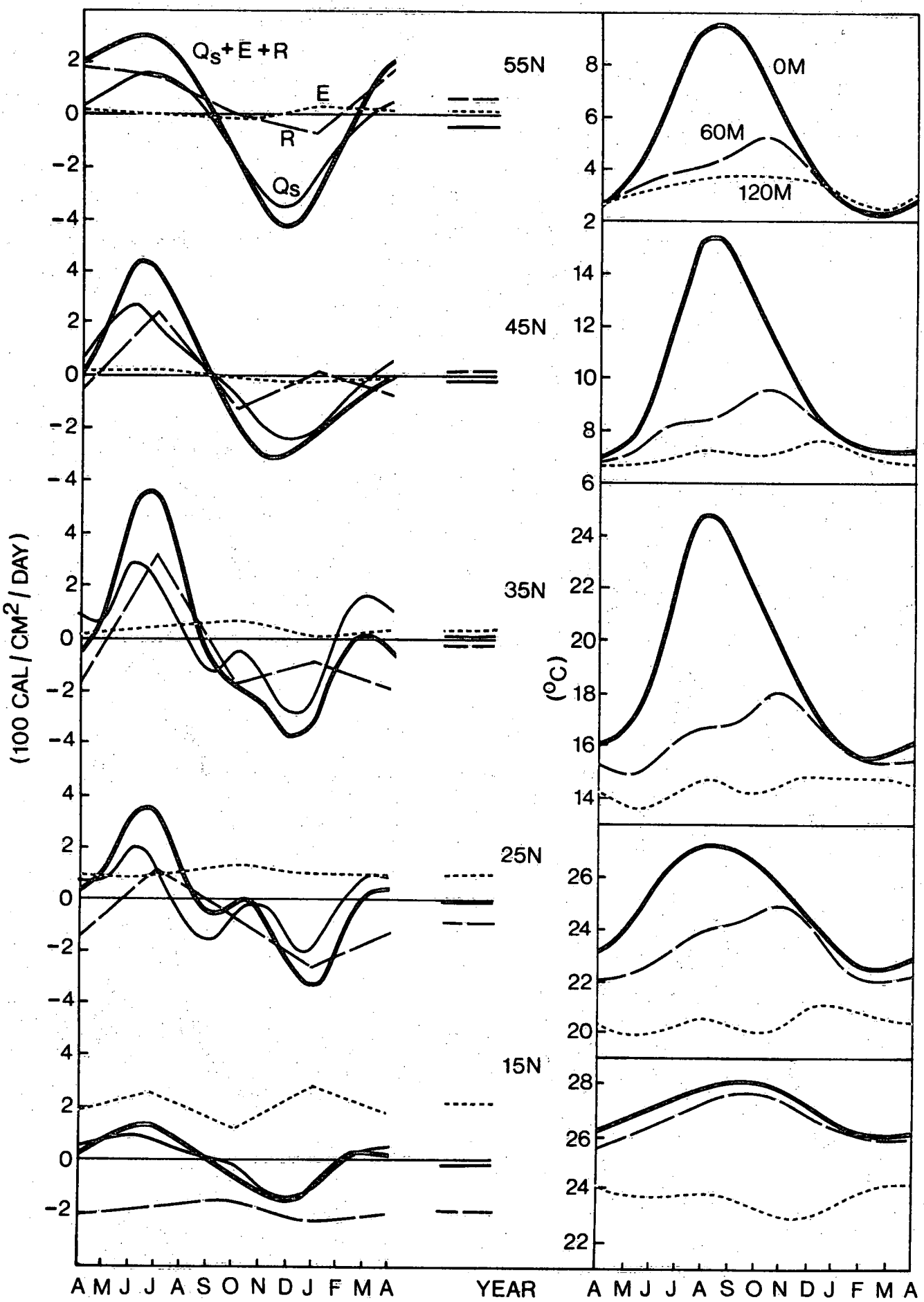
Qs+E+R
E
R
Qs
55N
45N
35N
25N
15N
0M
60M
120M
(100 CAL / CM2 / DAY)
(°C)
A M J J A S O N D J F M A
YEAR
A M J J A S O N D J F M A

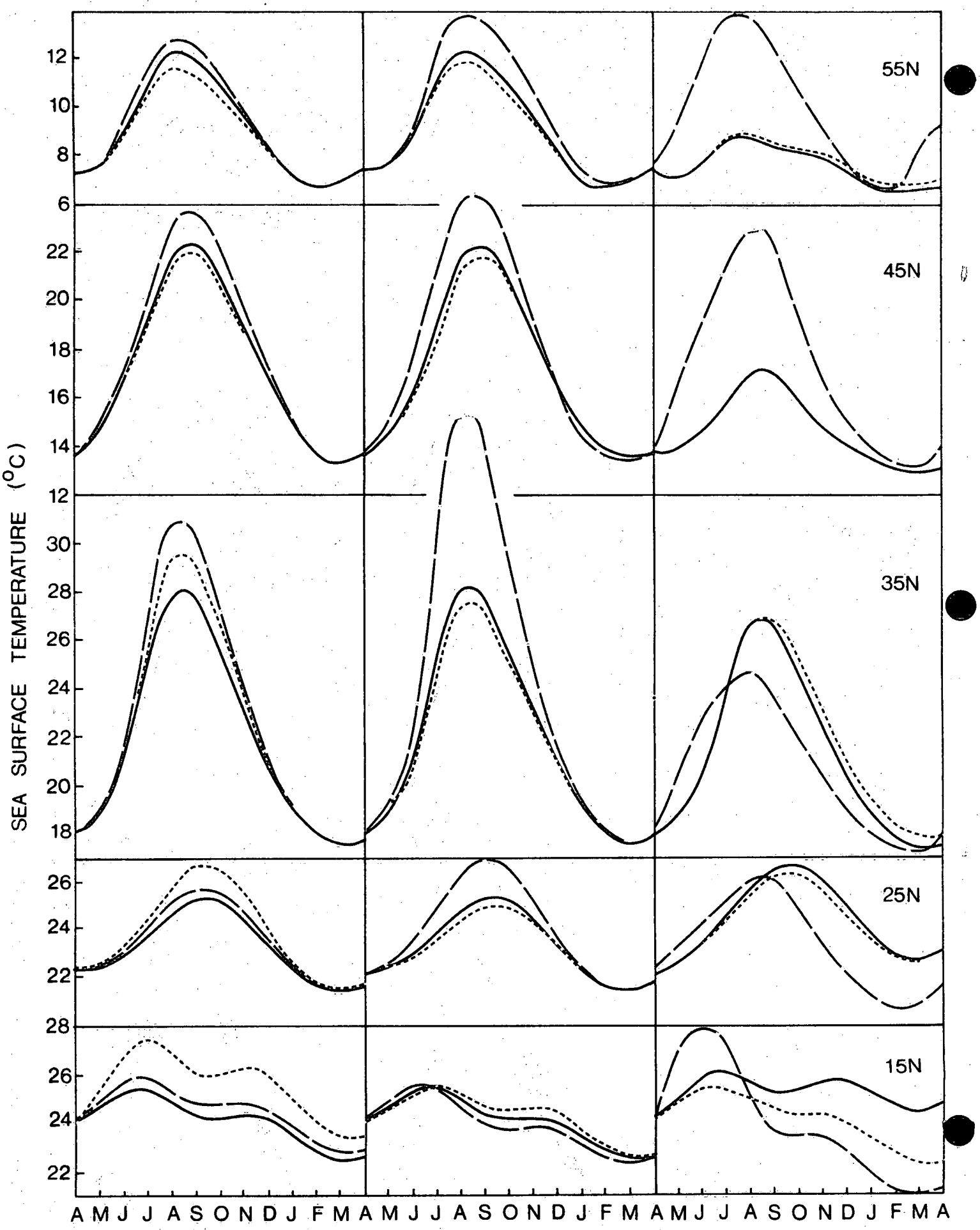
SEA SURFACE TEMPERATURE (°C)
55N
45N
35N
25N
15N
12
10
8
6
22
20
18
16
14
12
30
28
26
24
22
20
18
26
24
22
28
26
24
22
A M J J A S O N D J F M A M J J A S O N D J F M A M J J A S O N D J F M A

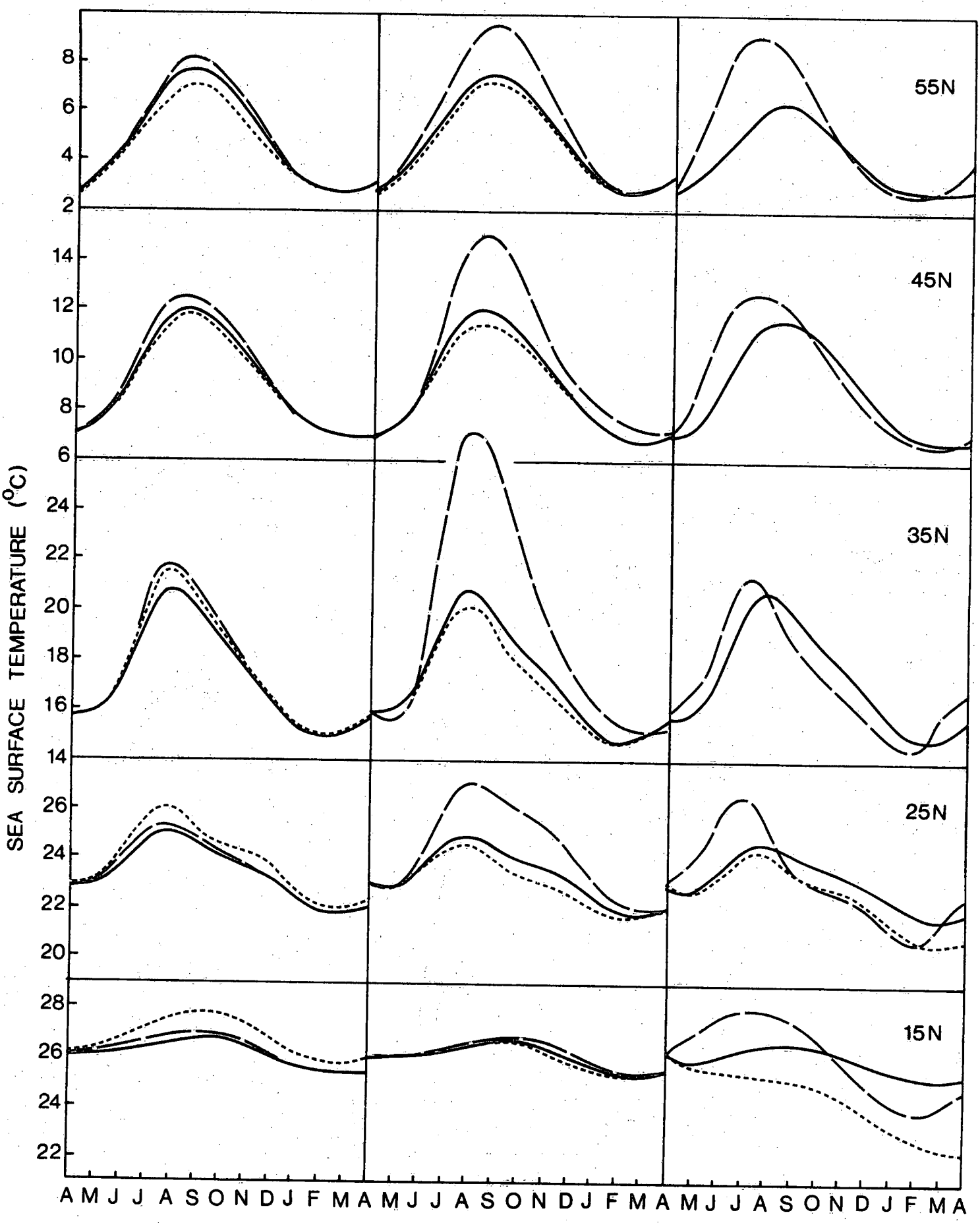
55N
45N
35N
25N
15N
SEA SURFACE TEMPERATURE (°C)
A M J J A S O N D J F M A M J J A S O N D J F M A M J J A S O N D J F M A

16005